



**MODELLING OF DYNAMICAL BEHAVIOR OF COMPOSITE MATERIALS  
WITH  
DISCONTINUOUS GALERKIN METHOD**

**Ph.D. Thesis by**

**Hüseyin Gökmen AKSOY, M.Sc.**

**Department : Mechanical Engineering**

**Programme : Mechanical Engineering**

**SEPTEMBER 2008**

**MODELLING OF DYNAMICAL BEHAVIOR OF COMPOSITE MATERIALS  
WITH  
DISCONTINUOUS GALERKIN METHOD**

**Ph.D. Thesis by**

**Hüseyin Gökmen AKSOY, M.Sc.**

**(503022017)**

**Date of submission : 29 April 2008**

**Date of defence examination : 9 September 2008**

**Supervisor (Chairman) : Assoc. Prof. Dr. Erol ŞENOCAK**

**Members of the Examining Committee Prof. Dr. Mehmet AKGÜN (Y.Ü.)**

**Prof. Dr. Mehmet DEMİRKOL (İ.T.Ü.)**

**Assoc. Prof. Dr. Şafak YILMAZ (İ.T.Ü.)**

**Prof. Dr. Yalçın AKÖZ (M.Ü.)**

**SEPTEMBER 2008**

**KOMPOZİT MALZEMELERİN  
SÜREKSİZ GALERKİN YÖNTEMİ İLE MODELLENMESİ**

**DOKTORA TEZİ**

**Y.Mak.Müh. Hüseyin Gökmen AKSOY**

**(503022017)**

**Tezin Enstitüye Verildiği Tarih : 29 Nisan 2008**

**Tezin Savunulduğu Tarih : 9 Eylül 2008**

**Tez Danışmanı : Doç. Dr. Erol ŞENOCAK**

**Diğer Jüri Üyeleri Prof. Dr. Mehmet AKGÜN (Y.Ü.)**

**Prof. Dr. Mehmet DEMİRKOL (İ.T.Ü.)**

**Doç. Dr. Şafak YILMAZ (İ.T.Ü.)**

**Prof. Dr. Yalçın AKÖZ (M.Ü.)**

**EYLÜL 2008**

## **ACKNOWLEDGEMENT**

I would like to thank to my supervisor Assoc. Prof. Dr. Erol Şenocak for his valuable help, patience and understanding in the course of this thesis work. In addition financial support of the Scientific and Technological Research Council of Turkey through out this thesis study is gratefully acknowledged. I would like to give special thanks to my mother to whom this thesis work is dedicated.

September 2008

Hüseyin Gökmen AKSOY

## TABLE OF CONTENTS

<b>ABBREVIATIONS</b>	<b>v</b>
<b>LIST OF TABLES</b>	<b>vi</b>
<b>LIST OF FIGURES</b>	<b>vii</b>
<b>LIST OF SYMBOLS</b>	<b>ix</b>
<b>SUMMARY</b>	<b>x</b>
<b>ÖZET</b>	<b>xi</b>
<b>1. Introduction</b>	<b>1</b>
1.1. Literature Survey	2
1.2. Objective and Research Methodology	4
<b>2. Governing Equations</b>	<b>6</b>
2.1. Equation of Motion	6
2.2. Theory on Discontinuous Surfaces	7
<b>3. Discretization</b>	<b>8</b>
3.1. Discontinuous Galerkin Method	8
<b>4. Numerical Implementation</b>	<b>13</b>
4.1. Spatial Discretization	13
4.2. Time Integration	14
4.2.1. Newmark Method	14
4.2.2. Time Discontinuous Galerkin Method	14
<b>5. Numerical Examples</b>	<b>16</b>
5.1. One Dimensional Examples	16
5.1.1. Shock Wave Propagation Problem	16
5.1.2. Bar impact on a rigid wall	17
5.1.3. Bi-material bar impact on a rigid wall	18
5.1.4. One Dimensional Wave Propagation in FGM	19
5.2. Two Dimensional Examples	22
5.2.1. Suddenly Loaded Axi-Symmetric Circular Plate	22
5.2.1.1. Forward Loaded Plate	23
5.2.1.2. Backward Loaded Plate	25
<b>6. CONCLUSIONS AND FUTURE WORK</b>	<b>27</b>
<b>APPENDIX</b>	<b>29</b>
<b>A. Figures</b>	<b>29</b>
<b>B. Kinematical Conditions of Compatibility</b>	<b>66</b>

<b>C. Balance Laws Around Discontinuous Surface</b>	<b>67</b>
<b>CIRRICULUM VITAE</b>	<b>69</b>

## ABBREVIATIONS

<b>DGM</b>	:	Discontinuous Galerkin Method
<b>TDG</b>	:	Time Discontinuous Galerkin
<b>FGM</b>	:	Functionally Graded Material
<b>PDE</b>	:	Partial Differential Equation
<b>FEM</b>	:	Finite Element Method
<b>CFL</b>	:	Courant Friedrichs Lewy Number $CFL = c\Delta t/\Delta x$



## LIST OF TABLES

	<u>Page No</u>
<b>Table 5.1</b> Total energy at $t = 8$ for DGM. . . . .	20
<b>Table 5.2</b> Total energy at $t = 8$ for stabilized DGM. . . . .	20
<b>Table 5.3</b> Material properties for layered bar. . . . .	21
<b>Table 5.4</b> Material properties of ceramic and metal phases of plate. . . .	22

## LIST OF FIGURES

	<u>Page No</u>
<b>Figure 2.1</b> : Typical domain having singular surface. . . . .	7
<b>Figure 3.1</b> : Typical solution domain and space-time slab. . . . .	9
<b>Figure A.1</b> : Initial displacement field for shock wave propagation problem. . . . .	29
<b>Figure A.2</b> : Conservation of energy for different mesh sizes ( $\Delta t = 0.002$ ). . . . .	30
<b>Figure A.3</b> : Variation of total energy for different time steps ( $N_e = 512$ ). . . . .	31
<b>Figure A.4</b> : Comparison of Newmark method and TDG for different time steps ( $N_e = 512$ ). . . . .	31
<b>Figure A.5</b> : Stress at $3^{rd}$ and $6^{th}$ periods for different methods. . . . .	32
<b>Figure A.6</b> : Bar impact on a rigid wall problem. . . . .	32
<b>Figure A.7</b> : $L_2$ norm of the error in displacement at different time steps at $t = 2$ for bar impact problem. . . . .	33
<b>Figure A.8</b> : Total energy variation at different time steps for bar impact problem. . . . .	34
<b>Figure A.9</b> : Comparison of the stress in the bar at $t = 5$ for bar impact problem. . . . .	35
<b>Figure A.10</b> : Bi-material bar impact on a rigid wall problem. . . . .	35
<b>Figure A.11</b> : $L_2$ norm of the error in displacement at different time steps at $t = 1.5$ for bi-material bar impact problem;(—: stabilized DGM, - - -: DGM). . . . .	36
<b>Figure A.12</b> : $L_2$ norm of the error in displacement at different time steps at $t = 4.5$ for bi-material bar impact problem;(—: stabilized DGM, - - -: DGM). . . . .	37
<b>Figure A.13</b> : Stress in the bar at $t = 1.5$ for bi-material bar impact problem( $N_e = 400$ , $p = 2$ ). . . . .	38
<b>Figure A.14</b> : Stress in the bar at $t = 1.5$ for bi-material bar impact problem( $N_e = 96$ , $p = 2$ ). . . . .	39
<b>Figure A.15</b> : Stress in the bar at $t = 4.5$ for bi-material bar impact problem( $N_e = 96$ , $\Delta t = 0.02$ ). . . . .	40
<b>Figure A.16</b> : One dimensional bar. . . . .	41
<b>Figure A.17</b> : Material properties along the bar. . . . .	41
<b>Figure A.18</b> : Results of different mesh sizes and time steps at point B; —: FGM, - - -:Layered. . . . .	41
<b>Figure A.19</b> : Variation of stress on the bar at different points. . . . .	42
<b>Figure A.20</b> : Variation of stress along the bar at different times. . . . .	43
<b>Figure A.21</b> : Axi-symmetric plate loaded from its center. . . . .	43
<b>Figure A.22</b> : Variation of volume fraction of ceramic phase among the thickness. . . . .	43
<b>Figure A.23</b> : Effective stress along the radius at $z/h = 0.625$ . . . . .	44
<b>Figure A.24</b> : Effective stress among the radius at $z/h = 0.375$ . . . . .	45
<b>Figure A.25</b> : Effective stress among the thickness at $r/R = 0.2$ . . . . .	46

<b>Figure A.26</b>	Effective stress among the thickness at $r/R = 0.8$ . . . . .	47
<b>Figure A.27</b>	$f_{rr}$ values at $r/R = 0.0$ . . . . .	48
<b>Figure A.28</b>	$f_{rr}$ values at $z/h = 0.5$ . . . . .	49
<b>Figure A.29</b>	$f_{zz}$ values at $r/R = 0.0$ . . . . .	50
<b>Figure A.30</b>	$f_{zz}$ values at $z/h = 0.5$ . . . . .	51
<b>Figure A.31</b>	$f_{rz}$ values at $r/R = 0.0$ . . . . .	52
<b>Figure A.32</b>	$f_{rz}$ values at $z/h = 0.5$ . . . . .	53
<b>Figure A.33</b>	Shear stress in the plate at $t = 5\mu sec$ and $t = 10\mu sec$ . . . . .	54
<b>Figure A.34</b>	Variation of volume fraction of ceramic phase among the thickness for backward loaded plate. . . . .	55
<b>Figure A.35</b>	Effective stress along the radius at $z/h = 0.625$ . . . . .	56
<b>Figure A.36</b>	Effective stress among the radius at $z/h = 0.375$ . . . . .	57
<b>Figure A.37</b>	Effective stress along the thickness at $r/R = 0.2$ . . . . .	58
<b>Figure A.38</b>	Effective stress among the thickness at $r/R = 0.8$ . . . . .	59
<b>Figure A.39</b>	$f_{rr}$ values at $r/R = 0.0$ . . . . .	60
<b>Figure A.40</b>	$f_{rr}$ values at $z/h = 0.5$ . . . . .	61
<b>Figure A.41</b>	$f_{zz}$ values at $r/R = 0.0$ . . . . .	62
<b>Figure A.42</b>	$f_{zz}$ values at $z/h = 0.5$ . . . . .	63
<b>Figure A.43</b>	$f_{rz}$ values at $z/h = 0.5$ . . . . .	64
<b>Figure A.44</b>	Shear stress in the plate at two different time. . . . .	65

## LIST OF SYMBOLS

$\rho$	: Density
$\mathbf{u}$	: Displacement vector
$\mathbf{v}$	: Velocity vector
$\mathbf{a}$	: Acceleration vector
$\mathbf{b}$	: Body force per unit volume
$\boldsymbol{\sigma}$	: Cauchy stress
$\varepsilon$	: Internal energy per unit volume
$\mathbf{q}$	: Heat flux
$\mathbf{g}$	: traction force at the Neumann boundary
$\mathbf{h}$	: Displacement at the boundary
$e_{ij}$	: Strain tensor
$\lambda, \mu$	: Lamé coefficients
$E$	: Young modulus
$\nu$	: Poisson ratio
$\Omega$	: Spatial domain
$\Gamma$	: Spatial domain boundary
$\Gamma_{int}$	: Interface between two elements
$\Gamma_N$	: Neumann boundary
$\Gamma_D$	: Dirichlet boundary
$S$	: Space-time domain
$\mathbf{c}$	: Velocity of discontinuity
$w$	: Weight function
$A(\cdot, \cdot)$	: Bilinear operator
$\mathbf{M}$	: Mass matrix
$\mathbf{K}$	: Stiffness matrix
$\Delta t$	: Time step
$\Delta x$	: Characteristic mesh size
$\gamma, \beta$	: parameters in the Newmark Algorithm
$f$	: Volume fraction of a material phase
$(\cdot)_S$	: Singular surface
$(\cdot)_e$	: Element of interest
$[\cdot]$	: Difference operator
$\langle \cdot \rangle$	: Average operator

# **MODELLING OF DYNAMICAL BEHAVIOR OF COMPOSITE MATERIALS WITH DISCONTINUOUS GALERKIN METHOD**

## **SUMMARY**

Modelling of dynamical behavior of materials takes attention of many researchers due to the industrial and military applications. Modelling of composite materials, which are used in military equipments, under impact loads gains importance. Time integration method used in dynamic problems has a significant effect on the results. Numerical dispersion and diffusion used in dynamic computational mechanics problems causes energy losses and oscillations. Thus it is possible to differ the energy losses and oscillations caused by the time integration. On the other hand it may be difficult to determine numerical diffusion and dispersion from the physical one for inelastic problems due to the physics of the problems. Selection of time integration problems for these problems is more important. Modelling of discontinuity due to the impact loads with continuous Galerkin method causes dispersion.

In this study time discontinuous Galerkin method and discontinuous Galerkin method are combined and reformulated to have a space-time discontinuous Galerkin method. This formulation is used in modelling of composite materials under impact loads. First numerical results are compared with analytical results of one dimensional problems for the determination of numerical properties of the formulation. Then the formulation is used to analyze one and two dimensional wave propagation in FGMs and layered materials. Results shows that space-time Galerkin method is successful in modelling composite materials under impact loads.

# **KOMPOZİT MALZEMELERİN SÜREKSİZ GALERKİN YÖNTEMİ İLE MODELLENMESİ**

## **ÖZET**

Malzemelerin dinamik davranışlarının modellenmesi farklı endüstriyel ve askeri uygulamalar nedeni ile birçok araştırmacının ilgisini çekmektedir. Özellikle askeri ekipmanlarda kullanılan kompozit malzemelerin ani darbe yükleri altındaki davranışı ve modellenmesi giderek önem kazanmaktadır. Dinamik problemlerin modellenmesinde kullanılan zaman integrasyonu sonucu önemli ölçüde etkilemektedir. Zaman ayrıklaştırmasında kullanılan yöntemden kaynaklanan sayısal yayılım ve dağılma, dinamik katı mekaniği problemlerinin sayısal çözümü sırasında, gerçekte olmayan, enerji kayıplarına veya salınımlarına sebep olmaktadır. Lineer elastik problemlerde, zaman ayrıklaştırmasından kaynaklanan enerji kayıpları ve salınımları belirlenebilmesine rağmen, lineer olmayan elastisite problemlerinde veya problemin fiziki nedeni ile enerji kayıplarının olduğu problemlerde (plastik şekil değişimi problemleri gibi) bu tespit zorlaşmaktadır. Bu tür problemlerin çözümünde kullanılacak olan zaman integrasyonu yönteminin seçimi önem kazanmaktadır. Malzemenin ani olarak yüklenmesine bağlı olarak malzeme içerisinde meydana gelen süreksizliğin modellenmesi sürekli Galerkin yöntemi ile yapıldığında sayısal dağılım meydana gelmektedir.

Bu çalışmada zaman süreksiz Galerkin yöntemi ve süreksiz Galerkin yöntemi birleştirilerek uzay-zaman süreksiz Galerkin yöntemi elde edilmiştir. Elde edilen formülasyonun sayısal özelliklerini belirlemek amacı ile bir boyutlu örnek problemler kullanılmış, elde edilen sonuçlar analitik çözümler ile karşılaştırılmıştır. Daha sonra elde edilen formülasyon FDM'lerde (Fonksiyonel Derecelendirilmiş Malzeme) ve çok katmanlı malzemelerde 1 boyutlu ve 2 boyutlu dalga yayılması problemlerini incelemek amacı ile kullanılmıştır. Sonuçlar uzay-zaman süreksiz Galerkin yönteminin darbe yükü uygulanmış kompozit malzemelerin modellenmesinde başarılı olduğunu göstermiştir.

## 1. Introduction

Composite materials have been used by the engineers. Thus by using proper combination of different materials one can produce a material with an improved thermal, acoustical, mechanical or electrical properties according to the needs in design. Composite materials can be classified in three groups, which are fibrous composites, laminated composites and particulate composites [?]. Many different approaches have been used for approximating the mechanical behavior of composite materials. In approximating the mechanical behavior of composite materials, determination of the effective material properties is the main interest of the researchers. Two main approaches has been used. One is the macromechanical approach in which the effective material properties are determined by using different methods in order to obtain homogeneous effective material properties [?]. The second one is micromechanical approach in which each material phase is modelled in detail [?, ?, ?]. The mechanical behavior of composite materials under static loads are well documented. On the other hand less is known about mechanical behavior of composites under dynamic loads.

In modelling the dynamical behavior of the materials different approaches have been used. First one is the Eulerian approach where the mesh is fixed in space and material is defined in each element or volume. The boundary of the material during the deformation is followed by different methods. In solid mechanics this approach is used for modelling high strain rate problems, like powder compaction under high strain rates. Second approach is Lagrangian approach, in which the mesh points are fixed to the material. Therefore it is advantageous to use this approach in solid mechanics problems. Thus modelling the problem with this approach leads to large errors in high strain rate problems. Third one is the Arbitrary Lagrangian-Eulerian approach in which the boundary of the material domain is followed by means of Lagrangian approach and mesh points inside the material domain moves with a spring mass analogy and solution is done in

an Eulerian manner. In this approach, even there are deformation rates, the mesh does not deform too much. Therefore numerical error due to the mesh deformation is not very big. The fourth one is to use Lagrangian and Eulerian codes depending on the behavior of the materials. The reader can consult to Ref. [?] for the details of the approaches.

Modelling of shock wave propagation in solid mechanics is one of the major research area in modelling the dynamic behavior of materials. Wave propagation in composite materials are the main interests of the researchers. From early detection of earthquakes to medical diagnosis of human body needs studies on wave propagation in elastic media [?]. Two main issues become important within this context computational modelling of wave propagation. One is the wave propagation in layered media, the other is the time integration. In this study elastic wave propagation in composite materials is modelled by using space-time discontinuous Galerkin method which is developed by the author.

## **1.1 Literature Survey**

Two main approaches has been used in designing the composite plates. One is to use layered composite plates consisting of several layers made of different materials. Second one is to use FGMs.

In modelling the layered media most of the attention is paid to the defining the effective material properties. Many theoretical and experimental studies have been done on this topic [?, ?]. The reader can consult to the recent review on defining the effective material properties of laminated composite plates by Ref. [?]. The use of layered media in designing composite plates has some disadvantages. Sudden change in material properties causes stress concentration in the material [?] which may cause failure. FGMs have begun to be used in engineering designs in which the material properties vary gradually [?]. Therefore no stress concentration occurs due to sudden change of material properties. These properties makes the FGMs attractive for many applications. Many researchers has begun to study on modelling the mechanical behaviour of FGMs. FEM is used for modelling the behaviour of FGM under suddenly applied loads [?] in which it is assumed that material properties vary linearly. Different models are compared



in determining the effective material properties for modelling composites [?]. It is concluded that materials with gradually changing material properties are more suitable for material problems in which the amplitude of the stress plays the key role. Researchers are focused on dynamical behavior of the layered metal-ceramic composites and composites with randomly embedded ceramic particles in a metal matrix [?]. It is seen that in the FGM the gradual change of material properties gives more physical results than using average material properties [?]. Plate impact experiments are made on aluminum nitride ceramic tiles bonded with thin silicon rubber at velocities ranging from 14-58 m/sec in Ref. [?]. Results are compared with the analytical solution. They concluded that the pulse is spreaded radially by the flexural waves.

Modelling of both FGMs and layered media are challenging task. Modelling of graded material increases the computational cost whilst modelling the layered media degrades the accuracy due to the sudden change of material properties. Degradation of numerical accuracy affects the conservation of energy, momentum and angular momentum. Conservation properties of numerical methods are important for the problems of solid dynamics, e.g., impact problems, plastic deformation problems. In recent years, the research on the conservative numerical methods for time integration and spatial discretization is getting more attention.

In the field of computational mechanics researchers have focussed on the conservation properties and stability of the time integration algorithms. Newmark time integration method [?] is one of the most widely used time integration method in structural dynamics. On behalf of this, Newmark family of algorithms are not energy and angular momentum conserving [?]. Energy preserving algorithms are developed by researchers [?]. Thus energy preserving schemes are lack off high frequency dissipation [?], which is necessary for damping high frequency oscillations in the numerical solution. Space-time finite element method is attractive for researchers due to the stability properties [?]. On the other hand time finite element methods are not energy conserving [?]. One approach in discretizing the balance equations is discontinuous Galerkin method [?]. Time Discontinuous Galerkin method (TDG) has begun to be used in elastodynamics [?]. It has small phase error and small dissipation error at high frequency regime

which damps the high frequency oscillations in the numerical solution [?]. This makes TDG attractive for wide range of structural problems. Straight forward implementation of TDG may cause problems. Therefore different algorithms are proposed by the researchers [?, ?, ?, ?] for the implementation.

Theoretical and numerical studies, in modelling of problems with discontinuities, in the variational framework goes back to 70's in solid dynamics [?, ?]. More recently the use of space-time discontinuous Galerkin method for shock wave propagation problems is proposed in References [?, ?, ?] for solid dynamics. Discontinuous Galerkin method (DGM) is widely used in fluid mechanics problems in discretizing first order partial differential equations (PDEs) due to its local and global conservation properties for spatial and temporal discretization [?]. As it allows discontinuities at the element interfaces it is advantageous to use DGM for shock wave propagation problems. More recently DGM for the discretization of second order PDEs has been developed [?, ?]. Comparison of different approaches used to discretize second order PDEs with DGM can be found in the literature [?, ?]. Another advantage of the DGM is continuously changing material properties can be defined in an element for FGMs and sudden change of the material properties are allowed at the element interfaces for layered materials.

## **1.2 Objective and Research Methodology**

The aim of this study is to develop a numerical method for modelling the shock wave propagation problems in composite materials for the comparison of the dynamical behaviour of layered composites and composites with gradually changing material properties under impact loads. For this purpose in the present study, author combined the time discontinuous Galerkin (TDG) presented in Ref. [?] and space discontinuous Galerkin presented in Ref. [?] in order to have space-time formulation. One and two dimensional computer codes are developed and validated for this purpose. Energy conservation properties of this formulation is analyzed for one dimensional problems [?]. Space-time discontinuous Galerkin formulation is used for modelling FGMs and layered materials which is proposed in Ref. [?].

One dimensional case studies with known exact solutions are carried out to determine the characteristics of the formulation. Two of the shock wave propagation problems are selected. One dimensional single material, and bi-material bar impacting on a rigid wall are chosen as case studies. Numerical results are compared to those of the known exact solutions of the problems to determine the numerical properties of the formulation. Lagrange polynomials are used for both space and time as basis functions. Then shock wave propagation problem is studied on  $1D$  bar suddenly loaded from its end for the comparison of layered and FGM material. Numerical results are compared with the analytical results given in Ref. [?]. Two dimensional axi-symmetric plate is also studied for the comparison of layered material and FGM.

## 2. Governing Equations

### 2.1 Equation of Motion

Cauchy equation of motion can be written as follows.

$$\rho \ddot{\mathbf{u}} - \nabla \cdot \boldsymbol{\sigma} - \rho \mathbf{b} = 0 \quad \text{in } \Omega \times I \quad (2.1)$$

In the equation above, upper dot represents the derivation with respect to time.  $\mathbf{u}$  is displacement,  $\boldsymbol{\sigma}$  is Cauchy stress tensor,  $\rho$  is density and  $\mathbf{b}$  represents the body forces.

Boundary conditions can be defined as follows.

$$\begin{aligned} \boldsymbol{\sigma} \cdot \mathbf{n} &= \mathbf{g} & \text{in } \Gamma_N \\ \mathbf{u} &= \mathbf{h} & \text{in } \Gamma_D \end{aligned} \quad (2.2)$$

For a linear elastic, isotropic material stress tensor can be defined as follows for small displacements.

$$\sigma_{ij} = [\lambda \delta_{ij} \delta_{km} + \mu (\delta_{ik} \delta_{jm} + \delta_{im} \delta_{jk})] e_{km} \quad (2.3)$$

In Equation (2.3)  $\lambda$  and  $\mu$  are Lamé coefficients.  $\delta$  is kroneckerdelta. Strain tensor  $e_{ij}$  is given in Equation (2.4) for small strains.

$$e_{ij} = \frac{1}{2} \left( \frac{\partial u_i}{\partial x_j} + \frac{\partial u_j}{\partial x_i} \right) \quad (2.4)$$

Equation of motion can be written as follows for a one dimensional problem.

$$\rho u_{,tt} - E u_{,xx} = 0 \quad (2.5)$$

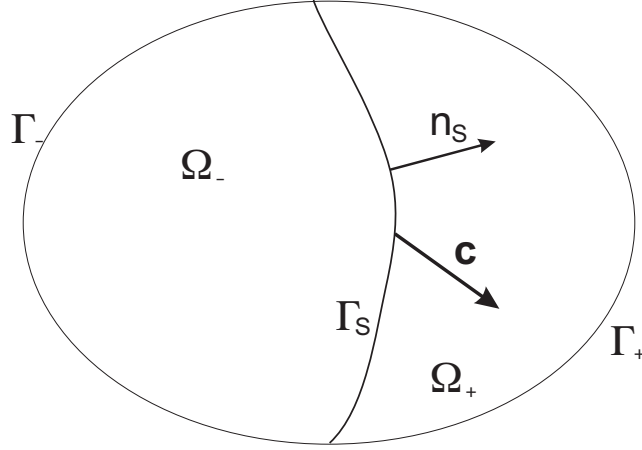


**Figure 2.1:** Typical domain having singular surface.

## 2.2 Theory on Discontinuous Surfaces

The equation motion given in the previous section is valid when the displacement, velocity and stress is smoothly varying. If there is a discontinuous surface in the material domain  $\Omega$ , then kinematical conditions of compatibility and local balance laws are valid around discontinuous surface.

The kinematical condition of compatibility can be written as follows.

$$[\mathbf{v}] + c_n [\nabla \mathbf{u}] \cdot \mathbf{n}_S = 0 \quad (2.6)$$

The local balance laws around a shock wave can be written as follows:

$$\begin{aligned} \text{Mass balance} & : [\rho(\mathbf{v} - \mathbf{c})] \cdot \mathbf{n}_S \\ \text{Momentum balance} & : [\rho \mathbf{v} (\mathbf{v} - \mathbf{c})] \cdot \mathbf{n}_S - [\boldsymbol{\sigma}] \cdot \mathbf{n}_S \\ \text{Energy balance} & : [(\rho \varepsilon + \frac{1}{2} \mathbf{v} \cdot \mathbf{v})(\mathbf{v} - \mathbf{c})] \cdot \mathbf{n}_S = [\boldsymbol{\sigma} \cdot \mathbf{v} - \mathbf{q}] \cdot \mathbf{n}_S \end{aligned} \quad (2.7)$$

Details of derivation of the above equations are given in the appendices. Theory on discontinuities are well documented in References [?, ?].

### 3. Discretization

#### 3.1 Discontinuous Galerkin Method

Let  $\mathcal{P}_h(\Omega)$  is a regular partition of the domain  $\Omega$  such that  $\mathcal{P}_h(\Omega)$  is generated by division of  $\Omega$  in to  $N_e$  number of  $\Omega_e$  subdomains. Boundary of each subdomain  $\Omega_e$  is partially continuous arc for two dimensional problems and partially continuous surfaces for three dimensional problems.  $\Gamma_{int}$  defines the interelement boundaries. Let  $I_n = (t_n, t_{n+1})$ . Then each space-time slab can be defined as  $S = \Omega \times I_n$ .

Let us define broken space of trial functions  $\mathbf{V}_n$  in which  $\mathbf{u}(\mathbf{x}, t)$  and  $\mathbf{v}(\mathbf{x}, t)$  are smooth and continuous vector functions for every  $S_e = \Omega_e \times I_n$ . Similarly broken space of weighting functions  $\mathbf{W}_n$  in which  $\mathbf{w}(\mathbf{x}, t)_u$  and  $\mathbf{w}(\mathbf{x}, t)_v$  are smooth and continuous vector functions for every  $S_e = \Omega_e \times I_n$ . Elements of  $\mathbf{V}_n$  and  $\mathbf{W}_n$  are vector functions different than zero in  $S_e$  and zero elsewhere. Typical solution domain in space and space-time slab is shown in Figure (3.1).

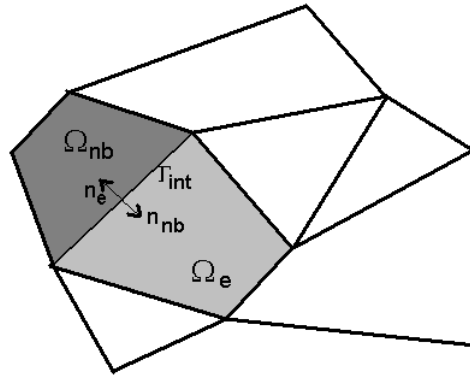
Weak formulation developed in Ref. [?] is adapted for solid dynamics and used for the discretization in space. The details of obtaining the bilinear and linear operator is given for the readers convenience. Let  $\mathbf{u}$  be the solution of the problem defined in Equations (2.1) and (2.2).

Difference and averaging operators can be defined as follows:

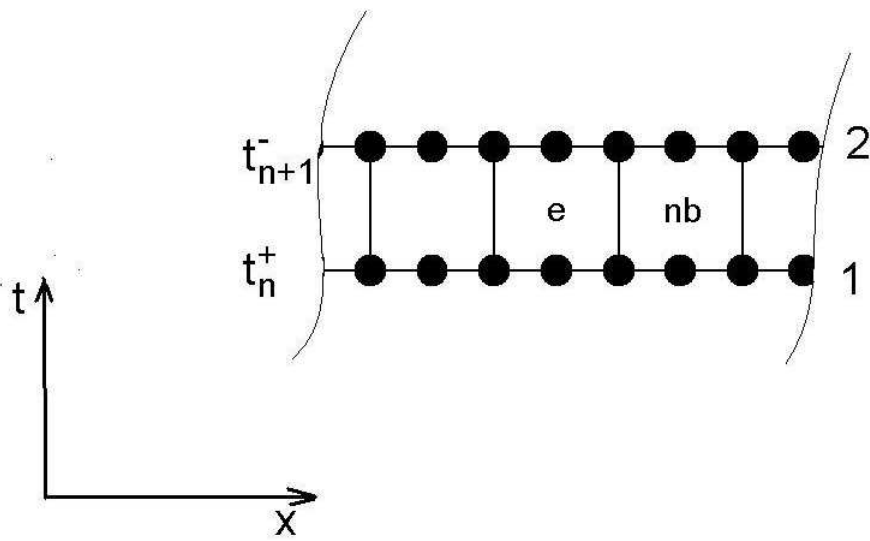
$$\begin{aligned} [\phi] &= (\phi_e - \phi_{nb}) \\ \langle \phi \rangle &= (\phi_e + \phi_{nb})/2 \end{aligned}$$

$$\sum_{\Omega_e \in \mathcal{P}_h} \int_{\Omega_e} w(\rho \ddot{\mathbf{u}} - \nabla \cdot \boldsymbol{\sigma} - \rho \mathbf{b}) dv = 0 \quad (3.1)$$

Where  $w$  is an arbitrary weighting function. Taking the second term and integrating by parts, we obtain the following equation.



(a) Solution domain



(b) Space-time slab

**Figure 3.1:** Typical solution domain and space-time slab.

$$-\int_{\Omega_e} w \nabla \cdot \boldsymbol{\sigma} dv = \sum_{\Omega_e} \left( -\int_{\Gamma_e} w \boldsymbol{\sigma} \cdot \mathbf{n}_e ds + \int_{\Omega_e} \nabla w \cdot \boldsymbol{\sigma} dv \right) \quad (3.2)$$

In Equation (3.2),  $\mathbf{n}_e$  is the unit outward vector. Thus one must note that  $\mathbf{n}_e = -\mathbf{n}_{nb} = \mathbf{n}$ . Rearranging the Equation (3.2), following equation is obtained.

$$\begin{aligned} \sum_{\Omega_e \in \mathcal{P}_h} \left( -\int_{\Gamma_e} w \boldsymbol{\sigma} \cdot \mathbf{n} ds + \int_{\Omega_e} \nabla w \cdot \boldsymbol{\sigma} dv \right) = & -\int_{\Gamma_{int}} [w \boldsymbol{\sigma}] \cdot \mathbf{n} ds \\ & -\int_{\Gamma_D} w \boldsymbol{\sigma} \cdot \mathbf{n} ds \\ & -\int_{\Gamma_N} w \mathbf{g} ds \end{aligned} \quad (3.3)$$

Since  $a \cdot b - c \cdot d = (a - c)(b + d)/2 + (a + c)(b - d)/2$ , we can write the first term on the right hand side of the Equation (3.3) as follows.

$$\begin{aligned} -\int_{\Gamma_{int}} [w \boldsymbol{\sigma}] \cdot \mathbf{n} ds = & -\int_{\Gamma_{int}} \langle w \rangle [\boldsymbol{\sigma}] \cdot \mathbf{n} ds \\ & -\int_{\Gamma_{int}} [w] \langle \boldsymbol{\sigma} \rangle \cdot \mathbf{n} ds \end{aligned} \quad (3.4)$$

Second term on the right hand side vanishes due to the Newton's third law in Equation (3.4). Then Equation (3.3) takes the form below.

$$\begin{aligned} \sum_{\Omega_e \in \mathcal{P}_h} \left( -\int_{\Gamma_e} w \boldsymbol{\sigma} \cdot \mathbf{n}_e ds + \int_{\Omega_e} \nabla w \cdot \boldsymbol{\sigma} dv \right) = & -\int_{\Gamma_{int}} \langle w \rangle [\boldsymbol{\sigma}] \cdot \mathbf{n} ds \\ & -\int_{\Gamma_D} w \boldsymbol{\sigma} \cdot \mathbf{n} ds \\ & -\int_{\Gamma_N} w \mathbf{g} ds \end{aligned} \quad (3.5)$$

In order to have a well posed problem continuity of the displacements are satisfied in weak manner as follows.

$$\begin{aligned} \sum_{\Omega_e \in \mathcal{P}_h} \left( -\int_{\Gamma_e} w \boldsymbol{\sigma} \cdot \mathbf{n} ds + \int_{\Omega_e} \nabla w \cdot \boldsymbol{\sigma} dv \right) = & -\int_{\Gamma_{int}} [w] \langle \boldsymbol{\sigma} \rangle \cdot \mathbf{n} ds \\ & -\lambda \int_{\Gamma_{int}} \langle \boldsymbol{\sigma}(w) \rangle [\mathbf{u}] \cdot \mathbf{n} ds \\ & -\int_{\Gamma_D} w \boldsymbol{\sigma} \cdot \mathbf{n} ds \\ & -\int_{\Gamma_N} w \mathbf{g} ds \end{aligned} \quad (3.6)$$

Then one can write the bilinear and linear operators for spatial discretization as follows.

$$\begin{aligned} A(\mathbf{u}, w) = & \sum_{\Omega_e \in \mathcal{P}_h} \left\{ \int_{\Omega_e} \nabla w \cdot \boldsymbol{\sigma} d\Omega_e \right\} - \int_{\Gamma_{int}} [w] \langle \boldsymbol{\sigma} \rangle \cdot \mathbf{n} d\Gamma_{int} \\ & + \int_{\Gamma_{int}} \langle \boldsymbol{\sigma}(w) \rangle \cdot \mathbf{n} [\mathbf{u}] d\Gamma_{int} - \int_{\Gamma_D} w \boldsymbol{\sigma} \cdot \mathbf{n} d\Gamma_D + \int_{\Gamma_D} \boldsymbol{\sigma}(w) \cdot \mathbf{n} \mathbf{u} d\Gamma_D \end{aligned} \quad (3.7)$$

$$L(w) = \sum_{\Omega_e \in \mathcal{P}_h} \int_{\Omega_e} w \rho \mathbf{b} d\Omega_e + \sum_{\Gamma_e \in \Gamma_D} \int_{\Gamma_e} \boldsymbol{\sigma}(w) \cdot \mathbf{n} \mathbf{h} d\Gamma_e + \sum_{\Gamma_e \in \Gamma_N} \int_{\Gamma_e} w \mathbf{g} d\Gamma_e. \quad (3.8)$$



The stabilization terms developed in Ref. [?] is also added to the bilinear operator in order to improve the convergence. Then the resulting bilinear and linear operators are can be written as follows;

$$\begin{aligned}
A(\mathbf{u}, w) = & \sum_{\Omega_e \in \mathcal{P}_h} \left\{ \int_{\Omega_e} \nabla w \cdot \boldsymbol{\sigma} d\Omega_e \right\} \\
& - \int_{\Gamma_{int}} [w] \langle \boldsymbol{\sigma} \rangle \cdot \mathbf{n} d\Gamma_{int} \\
& + \int_{\Gamma_{int}} \langle \boldsymbol{\sigma}(w) \rangle \cdot \mathbf{n} [\mathbf{u}] d\Gamma_{int} \\
& - \int_{\Gamma_D} w \boldsymbol{\sigma} \cdot \mathbf{n} d\Gamma_D \\
& + \int_{\Gamma_D} \boldsymbol{\sigma}(w) \cdot \mathbf{n} \mathbf{u} d\Gamma_D \\
& + \mu \frac{\gamma_\mu}{h} \int_{\Gamma_{int}} [w] \cdot [\mathbf{u}] d\Gamma_{int} \\
& + \int_{\Gamma_{int}} \left[ \lambda \frac{\gamma_\lambda}{h} w \right] \cdot \mathbf{n} [\mathbf{u}] \cdot \mathbf{n} d\Gamma_{int} \\
& + \int_{\Gamma_D} \mu \frac{\gamma_\mu}{h} w \cdot \mathbf{u} d\Gamma_D \\
& + \int_{\Gamma_D} \lambda \frac{\gamma_\lambda}{h} w \cdot \mathbf{n} \mathbf{u} \cdot \mathbf{n} d\Gamma_D
\end{aligned} \tag{3.9}$$

$$\begin{aligned}
L(w) = & \sum_{\Omega_e \in \mathcal{P}_h} \int_{\Omega_e} w \rho \mathbf{b} d\Omega_e \\
& + \sum_{\Gamma_e \in \Gamma_D} \int_{\Gamma_e} \boldsymbol{\sigma}(w) \cdot \mathbf{n} \mathbf{h} d\Gamma_e \\
& + \sum_{\Gamma_e \in \Gamma_N} \int_{\Gamma_e} w \mathbf{g} d\Gamma_e
\end{aligned} \tag{3.10}$$

where,

$$\begin{aligned}
h &= 2 \left( \frac{\text{length}(\Gamma)}{\text{area}(\Omega_e)} + \frac{\text{length}(\Gamma)}{\text{area}(\Omega_{nb})} \right)^{-1} \quad \text{for } \Gamma \subset \Gamma_e \cap \Gamma_{nb} \\
h &= \frac{\text{area}(\Omega_e)}{\text{length}(\Gamma_e)} \quad \text{for } \Gamma \subset \Gamma_e \cap \partial\Omega
\end{aligned} \tag{3.11}$$

In Equation (3.9),  $\gamma_\mu$  and  $\gamma_\lambda$  are penalty parameters,  $\lambda$  and  $\mu$  are Lamè parameters.

Space-time discontinuous Galerkin formulation is finding  $\{\mathbf{u}, \mathbf{v}\} \in \mathbf{V}_n \times \mathbf{V}_n$  such that for all  $\{w_u, w_v\} \in \mathbf{W}_n \times \mathbf{W}_n$  based on two field formulation [?]. Two field formulation consists of momentum equation and definition of velocity.

$$\begin{aligned}
& \int_{I_n} \int_{\Omega_e} \mathbf{w}_v \rho \dot{\mathbf{v}} d\Omega_e dt + \int_{I_n} A(\mathbf{u}, \mathbf{w}_v) dt - \int_{I_n} L(\mathbf{w}_v) dt \\
& + \int_{I_n} A(\dot{\mathbf{u}}, \mathbf{w}_u) dt - \int_{I_n} A(\mathbf{v}, \mathbf{w}_u) dt = 0
\end{aligned} \tag{3.12}$$

Now let us take the first and fourth terms in Equation (3.12) and apply integration by parts.

$$\begin{aligned}
& \int_{I_n} \int_{\Omega_e} \mathbf{w}_v \rho \dot{\mathbf{v}} d\Omega_e dt = \int_{\Omega_e} \mathbf{w}_v \rho \mathbf{v} d\Omega_e \Big|_{t_n}^{t_{n+1}} - \int_{I_n} \int_{\Omega_e} \dot{\mathbf{w}}_v \rho \mathbf{v} d\Omega_e dt \\
& \int_{I_n} A(\dot{\mathbf{u}}, \mathbf{w}_u) dt = A(\mathbf{u}, \mathbf{w}_u) \Big|_{t_n}^{t_{n+1}} - \int_{I_n} A(\mathbf{u}, \dot{\mathbf{w}}_u) dt
\end{aligned} \tag{3.13}$$

Let  $\mathbf{u}^h$  and  $\mathbf{v}^h$  be the approximate solution of the problem defined by Equations (2.1) and (2.2). Then one can write the following equalities.

$$\begin{aligned}\mathbf{u} &= \mathbf{u}^h + \mathbf{e}_u \\ \mathbf{v} &= \mathbf{v}^h + \mathbf{e}_v\end{aligned}\tag{3.14}$$

In Equation (3.14)  $\mathbf{e}_u$  and  $\mathbf{e}_v$  are errors in approximating  $\mathbf{u}$  and  $\mathbf{v}$  respectively.

Substituting Equations (3.14) and (3.13) in Equation (3.12), we get the following equation.

$$\begin{aligned}& \int_{\Omega_e} \mathbf{w}_v \rho \mathbf{v}^h dv \Big|_{t_n}^{t_{n+1}} + \int_{\Omega_e} \mathbf{w}_v \rho \mathbf{e}_v dv \Big|_{t_n}^{t_{n+1}} \\& - \int_{I_n} \int_{\Omega_e} \dot{\mathbf{w}}_v \rho \mathbf{v}^h dv dt - \int_{I_n} \int_{\Omega_e} \dot{\mathbf{w}}_v \rho \mathbf{e}_v dv dt \\& + \int_{I_n} A(\mathbf{u}^h, \mathbf{w}_v) dt + \int_{I_n} A(\mathbf{e}_u, \mathbf{w}_v) dt \\& - \int_{I_n} L(\mathbf{w}_v) dt \\& + A(\mathbf{u}^h, \mathbf{w}_u) \Big|_{t_n}^{t_{n+1}} + A(\mathbf{e}_u, \mathbf{w}_u) \Big|_{t_n}^{t_{n+1}} \\& - \int_{I_n} A(\mathbf{u}^h, \dot{\mathbf{w}}_u) dt - \int_{I_n} A(\mathbf{e}_u, \dot{\mathbf{w}}_u) dt \\& - \int_{I_n} A(\mathbf{v}^h, \mathbf{w}_u) dt - \int_{I_n} A(\mathbf{e}_v, \mathbf{w}_u) dt = 0\end{aligned}\tag{3.15}$$

Applying integration by parts once more to the thirth and ninth terms in Equation (3.15) and assuming the error is zero, the following equation is obtained.

$$\begin{aligned}& \int_{\Omega_e} \mathbf{w}_v \rho \mathbf{v}^h dv \Big|_{t_n}^{t_{n+1}} - \int_{\Omega_e} \mathbf{w}_v \rho \mathbf{v}^h dv \Big|_{t_n^+}^{t_{n+1}^-} \\& + \int_{I_n} \int_{\Omega_e} \mathbf{w}_v \rho \mathbf{v}^h dv dt \\& + \int_{I_n} A(\mathbf{u}^h, \mathbf{w}_v) dt \\& - \int_{I_n} L(\mathbf{w}_v) dt \\& + A(\mathbf{u}^h, \mathbf{w}_u) \Big|_{t_n}^{t_{n+1}} - A(\mathbf{u}^h, \mathbf{w}_u) \Big|_{t_n^+}^{t_{n+1}^-} \\& + \int_{I_n} A(\mathbf{u}^h, \dot{\mathbf{w}}_u) dt \\& - \int_{I_n} A(\mathbf{v}^h, \mathbf{w}_u) dt = 0\end{aligned}\tag{3.16}$$

Assuming that  $\mathbf{u}(t_{n+1}^-)$  is the exact solution of the problem defined in Equation (2.1), the solution of the Equation (3.17) is the solution of the problem defined in Equation (2.1) and Equation (2.2).

$$\begin{aligned}& \int_{I_n} \int_{\Omega_e} \mathbf{w}_v \rho \dot{\mathbf{v}} d\Omega_e dt + \int_{I_n} A(\mathbf{u}^h, \mathbf{w}_v) dt - \int_{I_n} L(\mathbf{w}_v) dt \\& + \int_{I_n} A(\mathbf{u}^h, \mathbf{w}_u) dt - \int_{I_n} A(\mathbf{v}^h, \mathbf{w}_u) dt \\& + \int_{\Omega_e} \mathbf{w}_v(t_n^+) \rho (\mathbf{v}^h(t_n^+) - \mathbf{v}^h(t_n^-)) d\Omega_e \\& + A(\mathbf{u}^h(t_n^+), \mathbf{w}_u(t_n^+)) - A(\mathbf{u}^h(t_n^-), \mathbf{w}_u(t_n^+)) \\& = A(\mathbf{u}^h(0^+), \mathbf{w}_u(0^+)) + \int_{\Omega_e} \mathbf{w}_v(0^+) \rho (\mathbf{v}^h(0^+)) d\Omega_e\end{aligned}\tag{3.17}$$

In Equation (3.17)  $\mathbf{w}_v$  and  $\mathbf{w}_u$  are the weight functions regarding to the momentum equation and definition of velocity respectively.

## 4. Numerical Implementation

Numerical implementation of Equation (3.17) is done first by discretizing the momentum equation in space by using the bilinear and linear operators which are given in Equation (3.7) and Equation (3.8). Then the resulting systems of ordinary differential equations are solved by using TDG.

Bilinear interpolation functions are used for the variation of material properties in an element for FGM.

### 4.1 Spatial Discretization

Bilinear operator can be written as follows after evaluating the integrals;

$$A(\mathbf{u}^{(he)}(t, \mathbf{X}), w) = \sum_{e=1}^{N_e} (\mathbf{K}_e \mathbf{u}(\mathbf{t})_e - \mathbf{F}_e(\mathbf{u}(\mathbf{t})_e) - \mathbf{F}_{nb}(\mathbf{u}(\mathbf{t})_{nb})). \quad (4.1)$$

In the above equation,  $\mathbf{K}_e$  is the element stiffness matrix.  $\mathbf{F}_e$  and  $\mathbf{F}_{nb}$  arises from the surface integrals along the element boundaries and can be regarded as force vectors acting on the surface of the element due to the displacement field inside the element and the displacement field from the neighbor element respectively. Body forces and boundary integrals subject to the boundary conditions can be written as

$$\sum_{e=1}^{N_e} \mathbf{F}_b = \sum_{\Omega_e \in \mathcal{P}_h} \int_{\Omega_e} w \rho \mathbf{b} dv + \lambda \sum_{\Gamma_e \in \Gamma_D} \int_{\Gamma_e} \nabla w \cdot \mathbf{n} \mathbf{h} dS + \sum_{\Gamma_e \in \Gamma_N} \int_{\Gamma_e} w \mathbf{g} dS. \quad (4.2)$$

Then one can write semi discrete balance equation as follows,

$$\sum_{e=1}^{N_e} (\mathbf{M}_e \ddot{\mathbf{u}}_e + \mathbf{K}_e \mathbf{u}_e - \mathbf{F}_e(\mathbf{u}_e) - \mathbf{F}_{nb}(\mathbf{u}_{nb}) - \mathbf{F}_{ext}) = 0. \quad (4.3)$$

In the above equations  $\mathbf{M}_e$  is the element mass matrix. The semi discrete balance equation can be written in a more compact form;

$$\sum_{e=1}^{N_e} (\mathbf{M}_e \ddot{\mathbf{u}}_e^{k+1} + \tilde{\mathbf{K}}_e \mathbf{u}_e^{k+1} - \mathbf{F}_{ext}^k) = 0. \quad (4.4)$$

The above equation can be solved element by element by using block Gauss-Seidell method along with the time integration method [?]. In the above equation superscript  $k$  is the iteration index in the Gauss-Seidell method.  $\mathbf{F}_{\text{ext}} = \mathbf{F}_b + \mathbf{F}_{nb}$  and modified element stiffness matrix is  $\tilde{\mathbf{K}}_e = \mathbf{K}_e + \frac{\partial \mathbf{F}_e}{\partial \mathbf{u}_e}$ .

## 4.2 Time Integration

### 4.2.1 Newmark Method

In Newmark time integration method, displacements and velocities are calculated by using Equations (4.5) in time interval  $I \in (t_{n+1}, t_n)$ .

$$\begin{aligned} u_{n+1} &= u_n + v_n \Delta t + \frac{\Delta t^2}{2} [(1 - 2\beta)a_n + 2\beta a_{n+1}] \\ v_{n+1} &= v_n + \Delta t [(1 - \gamma)a_n + \gamma a_{n+1}] \end{aligned} \quad (4.5)$$

Applying Newmark method to Equation (4.4), we get following equations for the displacements and velocities,

$$\begin{aligned} (\mathbf{I} + \Delta t \beta \mathbf{M}^{-1} \tilde{\mathbf{K}}) \mathbf{u}_{n+1}^{k+1} &= \mathbf{u}_n + \mathbf{v}_n \Delta t + \frac{\Delta t^2}{2} [(1 - 2\beta) \mathbf{a}_n + 2\beta \mathbf{M}^{-1} \mathbf{F}_{n+1}^k] \\ \mathbf{v}_{n+1} &= \mathbf{v}_n + \Delta t [(1 - \gamma) \ddot{\mathbf{u}}_n + \gamma \ddot{\mathbf{u}}_{n+1}^{k+1}]. \end{aligned}$$

Here  $n$  denotes the time level. In equations above and hereafter subscripts of the vectors and matrices are dropped for the simplicity. For the following section no subscript will be used to show element wise values.

### 4.2.2 Time Discontinuous Galerkin Method

Time discontinuous Galerkin (TDG) is used for the time integration. In the application of TDG double field formulation is used. Double field formulation consist of definition of velocity and equation of motion [?].

$$\begin{aligned} \int_I \mathbf{w}_t \left( \begin{bmatrix} \tilde{\mathbf{K}} & 0 \\ 0 & \mathbf{M} \end{bmatrix} \begin{bmatrix} \dot{\mathbf{u}} \\ \dot{\mathbf{v}} \end{bmatrix} + \begin{bmatrix} 0 & -\tilde{\mathbf{K}} \\ \tilde{\mathbf{K}} & 0 \end{bmatrix} \begin{bmatrix} \mathbf{u} \\ \mathbf{v} \end{bmatrix} \right) dt \\ + \mathbf{w}_t(t_n^+) \begin{bmatrix} \tilde{\mathbf{K}} & 0 \\ 0 & \mathbf{M} \end{bmatrix} \begin{bmatrix} \mathbf{u}(t_n^+) \\ \mathbf{v}(t_n^+) \end{bmatrix} - \mathbf{w}_t(t_n^+) \begin{bmatrix} \tilde{\mathbf{K}} & 0 \\ 0 & \mathbf{M} \end{bmatrix} \begin{bmatrix} \mathbf{u}(t_n^-) \\ \mathbf{v}(t_n^-) \end{bmatrix} &= \int_I \mathbf{w}_t \begin{bmatrix} 0 \\ \mathbf{F} \end{bmatrix} dt. \end{aligned} \quad (4.6)$$

In equations above subscripts of the vectors and matrices are dropped for the simplicity. For the following section no subscript will be used to show element wise

values. In Equation (4.6)  $\mathbf{w}_t$  is the weight function in time. 1<sup>st</sup> order Lagrange polynomials are used as a base function in time. After evaluating the integrals in Equation (4.6), one can obtain to the following linear equation system.

$$\begin{bmatrix} \frac{1}{2}\tilde{\mathbf{K}} & \frac{1}{2}\tilde{\mathbf{K}} & \frac{-1}{3}\text{dt}\tilde{\mathbf{K}} & \frac{1}{6}\text{dt}\tilde{\mathbf{K}} \\ \frac{-1}{2}\tilde{\mathbf{K}} & \frac{1}{2}\tilde{\mathbf{K}} & \frac{-1}{6}\text{dt}\tilde{\mathbf{K}} & \frac{-1}{3}\text{dt}\tilde{\mathbf{K}} \\ \frac{1}{3}\text{dt}\tilde{\mathbf{K}} & \frac{1}{6}\text{dt}\tilde{\mathbf{K}} & \frac{1}{2}\mathbf{M} & \frac{1}{2}\mathbf{M} \\ \frac{1}{6}\text{dt}\tilde{\mathbf{K}} & \frac{1}{3}\text{dt}\tilde{\mathbf{K}} & \frac{-1}{2}\mathbf{M} & \frac{1}{2}\mathbf{M} \end{bmatrix} \begin{bmatrix} \mathbf{u}_n^+ \\ \mathbf{u}_{n+1}^- \\ \mathbf{v}_n^+ \\ \mathbf{v}_{n+1}^- \end{bmatrix} = \begin{bmatrix} \tilde{\mathbf{K}}\mathbf{u}_n^- \\ 0 \\ \mathbf{F}_n + \mathbf{M}\mathbf{v}_n^- \\ \mathbf{F}_{n+1} \end{bmatrix} \quad (4.7)$$

Equation (4.7) is solved by using TGD-B algorithm proposed in Reference [?]. The detailed analysis of TDG and other time integration methods are done in References [?, ?].

## 5. Numerical Examples

### 5.1 One Dimensional Examples

#### 5.1.1 Shock Wave Propagation Problem

We first investigate the shock wave propagation problem on a bar with two ends fixed. In order to generate a shock wave initial displacement shown in Figure A.1 is given and initial velocity is taken as zero. The elasticity modulus, density and length of the bar is taken as unity. Computations are carried on different time steps ( $\Delta t = 0.02, 0.002$  and  $0.0002$ ) and element sizes ( $N_e = 64, 128, 256$  and  $512$ ). Second order Lagrange polynomials are used as a base functions for space discretization. Since the problem is periodic, computations are carried for 10 period of time. Convergence is obtained for all time steps and mesh sizes except from TDG with  $\Delta t = 0.02$ .

In Figure A.2 variation of total energy is shown for  $\Delta t = 0.002$  for Newmark method and TDG. As it is seen from the figure the increase in the number of the elements has a very little effect on the variation of the total energy.

In Figure A.3 variation of total energy is shown for  $N_e = 512$ . It is seen that with trapezoidal rule (Newmark method with  $\beta = 0.25, \gamma = 0.5$ ) the total energy does not change for all time steps. On the other hand when Newmark method with  $\beta = 0.5, \gamma = 1.0$  (hereafter will be called upwind method) is used, total energy decreases and when the time step is 0.02 the total energy of the system asymptotically decreases to zero. As the time step decreases the decay in total energy decreases. In TDG method the decay in total energy is %4 for  $\Delta t = 0.002$  and %1 for  $\Delta t = 0.0002$ .

In Figure A.4 Newmark method and TDG is compared for time steps  $\Delta t = 0.002$  and  $\Delta t = 0.0002$ . It is observed that total energy is conserved when trapezoidal

rule is used. On the other hand a decrease in total energy is seen when TDG and upwind method is used. This decrease is %4 of the initial total energy for TDG and %80 for the upwind method. As the time step decreases this ratio decreases up to %30 for the upwind method and %1 for TDG.

State of stress is shown in Figure A.5 at 3<sup>rd</sup> and 6<sup>th</sup> periods for different time integration methods. In trapezoidal rule the amplitude of the stress wave is approximately the same as the initial stress wave. Also very high dispersion is seen in the solution. In upwind method the shock is smeared and it turns to be a sinusoidal wave. In TDG high frequency oscillations are damped and wave shape is almost preserved.

### 5.1.2 Bar impact on a rigid wall

We compare the numerical solutions of a bar impact on a rigid wall, which is shown in Figure A.6. The length of the rod is  $L = 4$ . Elasticity modulus and density are taken as unity. Boundary conditions are  $u|_{x=0} = 0$ ,  $\frac{\partial u}{\partial x}|_{x=L} = 0$  and initial conditions are  $u(x, 0) = 0$ ,  $\dot{u}(x, 0) = -1$ .

Computational domain is divided into 400, 200, 100 and 50 three noded elements. Lagrange polynomials are used as a base function. Computations are carried on for three different time steps 0.02, 0.002 and 0.0002.

In Figures A.7 one can see the  $L_2$  norm of the error in displacement with number of elements  $N_e = 400$ . It is seen from the figures that convergence rates for TDG and trapezoidal rule (Newmark  $\beta=0.25$   $\gamma=0.5$ ) are very close except  $\Delta t = 0.02$ . For upwind method the norm of error is almost constant for different mesh sizes at  $\Delta t = 0.02$ . As the time step decreases also upwind time integration tends to have a linear convergence behavior.

In Figure A.8 total energy variations are shown. It is seen that total energy of the system is conserved when trapezoidal rule is used. High frequency oscillations are result of numerical dispersion in the solution. TDG and upwind methods are dissipative. Thus the decrease in energy in upwind method is %8 for  $\Delta t = 0.02$  and %0.75 for  $\Delta t = 0.0002$ , while it is %0.64 for  $\Delta t = 0.02$  and zero for  $\Delta t = 0.0002$  for TDG.

Stress variation in the bar is shown in Figure A.9. It is seen that trapezoidal rule is highly dispersive for all time steps. For TDG there are few oscillations are seen at the shockfront. As the time step decreases dispersion increases in TDG. For upwind method there is no oscillations seen in the stress except when  $\Delta t = 0.0002$ . Upwind solution gives less accurate solution around the shockfront.

### 5.1.3 Bi-material bar impact on a rigid wall

Bi-material bar impacting on a rigid wall is used as a second test case (see Fig. A.10). The same time steps are used as in the previous problem. The number of elements  $N_e = 48, 96, 200$  and  $400$  are used in the computations. CFL number varies between  $0.0034$  and  $2.8$ . Lagrange polynomials up to order of  $p = 4$  are used as basis functions. Density is taken as unity for all parts of the material. Elasticity modulus is  $E = 1$  for  $0 \leq x \leq 3/8L$  and  $E = 2$  for  $3/8L \leq x \leq L$ . The initial and boundary conditions are the same as the bar impact on rigid wall problem. Additional stabilization terms are used in the solution of this problem to determine the effect of stabilization terms. Penalty parameter  $\gamma_\mu$  is selected as 3 as proposed in Ref. [?]. Since the problem is one dimensional  $\lambda$  is zero, and the second penalty parameter  $\gamma_\lambda$  is not needed.

In Figure A.11,  $L_2$  norm of the error in displacements is shown for different orders ( $p$ ) of basis functions for different time steps. The curves of the diverged solutions are not shown in the figures. There is no converged result in the DGM for  $N_e = 200$  and  $N_e = 400$  at  $\Delta t = 0.02$ . It is determined that added stabilization terms decreases the magnitude of the error and improves the convergence. On the other hand, as the order of basis function increases, the solution diverges for some cases, shown in Figure A.11. As the time proceeds, divergence also occurs for some cases with stabilized DGM as seen in Figure A.12.

Stress variation is compared to the exact solution in Figures A.13 and A.14 for  $N_e = 400$  and  $N_e = 96$ , respectively. It is observed from the figures that as the time step decreases, dispersion in the numerical solution increases. The amplitude of the numerical oscillations decreases with the time step, whereas the affected area increases. The added stabilization term decreases the amplitude of the numerical



oscillations and affected region. Increase in the element number improves the resolution.

Stress in the bar is shown in Figure A.15 for  $N_e = 96$  and  $\Delta t = 0.02$  for different basis functions. In the figure, one can determine that as the order of polynomial increases, numerical oscillations decrease and shocks are captured more accurately. Also added stabilization terms improve the numerical solution significantly. Thus, very small numerical diffusion around shocks are seen when  $p = 4$  in numerical solution with the stabilized DGM.

Total energy values at  $t = 8$  are given in the Tables 5.1 and 5.2. Continuous lines in the tables represent the diverged solutions. Total energy of the system is 2 as in the first problem. It can be concluded from Table 5.1 that, when the time step is  $\Delta t = 0.02$ , energy decay is less than %1. In addition, as the number of elements increases energy decay also increases. The high values of total energy in the case of  $\Delta t = 0.0002$ , which are far from acceptable limits, are due to the divergence of the numerical solution. Also continuous lines in the tables show the diverged computations. One can see from the tables that the smaller is the time step, the smaller is the decay in total energy. Additional stabilization terms improve the convergency of the DGM. It is seen from Table 5.2 that the energy decay is higher in the computations with the stabilized DGM (compared to the DGM). On the other hand, it is observed that the total energy values do not change with the element number in the stabilized DGM and total energy does not change with the order of basis functions when the stabilized DGM is used. Therefore, it can be concluded that adding stabilization terms improves the conservation property of the DGM.

#### 5.1.4 One Dimensional Wave Propagation in FGM

In this section one dimensional bar suddenly loaded from its end with a 10kPa compression load is studied that is shown in Figure A.16. Poisson's ratio is taken as zero. Variation of Young's modulus and density for FGM is given in Equation (5.1). Variation of material properties along the bar is shown in Figure A.17. In Equation (5.1)  $E_0 = 100$  MPa and  $\rho_0 = 1$  Kg/m<sup>3</sup>. Material

**Table 5.1:** Total energy at  $t = 8$  for DGM.

		$p = 2$	$p = 3$	$p = 4$
$\Delta t = 0.02$	$N_e = 48$	1.9946	—	—
	$N_e = 96$	1.9883	1.9858	—
	$N_e = 200$	—	—	—
	$N_e = 400$	—	—	—
$\Delta t = 0.002$	$N_e = 48$	2.2635	—	—
	$N_e = 96$	2.1639	—	—
	$N_e = 200$	2.0047	—	—
	$N_e = 400$	1.9982	—	—
$\Delta t = 0.0002$	$N_e = 48$	2.2791	—	—
	$N_e = 96$	2.4985	—	—
	$N_e = 200$	12.6496	—	—
	$N_e = 400$	9109.3	—	—

**Table 5.2:** Total energy at  $t = 8$  for stabilized DGM.

		$p = 2$	$p = 3$	$p = 4$
$\Delta t = 0.02$	$N_e = 48$	1.9882	1.9857	—
	$N_e = 96$	1.9863	1.9858	—
	$N_e = 200$	1.9859	1.9858	—
	$N_e = 400$	1.9858	1.9858	—
$\Delta t = 0.002$	$N_e = 48$	2.0189	—	—
	$N_e = 96$	2.0026	—	—
	$N_e = 200$	1.9983	1.9974	1.9974
	$N_e = 400$	1.9976	1.9974	1.9974
$\Delta t = 0.0002$	$N_e = 48$	2.0244	—	—
	$N_e = 96$	2.0110	—	—
	$N_e = 200$	2.0067	—	—
	$N_e = 400$	2.0018	—	—

**Table 5.3:** Material properties for layered bar.

	Layer 1	Layer 2	Layer 3	Layer 4
Young Modulus (MPa)	103.411	110.789	119.005	128.19
Density (Kg/m <sup>3</sup> )	1.07154	1.235	1.4311	1.66799

properties for each layer is presented in Table 5.3. Bilinear basis functions are used. Penalty parameters  $\gamma_\mu$  and  $\gamma_\lambda$  selected to be 3.

$$\begin{aligned} E(x) &= E_0(ax/L + 1)^m \\ \rho(x) &= \rho_0(ax/L + 1)^n \end{aligned} \quad (5.1)$$

In Equation (5.1)  $L = 20m$ ,  $a = -0.14096$ ,  $m = -1.8866$  and  $n = -3.8866$ .

Numerical computations are made for three different time steps  $\Delta t = 1e-4$ ,  $\Delta t = 5e-5$  and  $\Delta t = 2.5e-5$  respectively. The bar is divided into  $N_e = 40$  and  $N_e = 160$  elements along its length. In Figure A.18 numerical results obtained for different number elements and time steps is shown at point A. It is observed that numerical results do not change significantly with the change of element and time step size. In case of  $\Delta t = 2.5e-5$  and  $N_e = 40$  the numerical solution does not converge for layered and FGM bar.

In Figure A.19 variation of stress at different points are shown. Both FGM and layered bar solutions are in close agreement with the analytical solution obtained for FGM apart from the step changes in stress for layered bar due to the sudden changes in material properties. On the other hand as the time proceeds the difference between the analytical solution and numerical results increases. Thus the analytical results are obtained for a short time. It is seen that solution obtained with layered bar is more oscillatory compared to the solution obtained from FGM bar. The amplitude of these oscillations are increasing as the time proceeds, which may lead to divergence. In addition phase difference occurs between FGM and layered bar. Also it is seen that the peak stresses are higher in FGM bar compared to the layered bar.

Variation of stress along the bar is shown in Figure A.20. It is seen that changes in the stress is more smooth in the numerical solution obtained for the FGM bar compared to the layered bar. The solution is oscillatory in the layered bar

**Table 5.4:** Material properties of ceramic and metal phases of plate.

	Young's modulus (GPa)	Poisson's ratio	Density (kg/m <sup>3</sup> )
Metal Matrix	70	0.3	2800
Ceramic	420	0.17	3200

compared to the FGM bar. It is also seen that state of the stress between FGM and layered bar differs significantly as time advances.

## 5.2 Two Dimensional Examples

### 5.2.1 Suddenly Loaded Axi-Symmetric Circular Plate

Two dimensional axi-symmetric metal-matrix composite plate, which is shown in Figure A.21, suddenly loaded from its center is studied for the comparison of FGMs and layered media for two dimensional problems. Therefore plate is divided into 4, 8 and 16 layers. The thickness of the plate is  $h = 0.02$  m and the radius is  $R = 0.1$  m. The load is applied up to the radius  $a = 0.005$  m from the center. The material properties of metal and ceramic phase, which is shown in table 5.4, is taken from Ref. [?]. Two different phase distribution is studied. One is forward loaded plates in which the ceramic phase is heavily concentrated in most part of the plate and later is backward loaded plate in which the aluminium phase is heavily concentrated in most part of the plate.

Numerical computations are carried out for three different time steps which are  $\Delta t = 0.2 \mu s$ ,  $\Delta t = 0.1 \mu s$  and  $\Delta t = 0.05 \mu s$ . The computational domain is divided into 1280, 5120 and 20480 quadratic equal sized elements. Bilinear basis functions are used. Penalty parameters are selected as  $\gamma_\mu = 3$  and  $\gamma_\lambda = 3$ . Grid convergence is achieved for all cases.

Effective stress  $\sigma_{eff.}$  values and its derivatives with respect to stress components( $f_{rr}$ ,  $f_{rz}$  and  $f_{zz}$ ) are compared. These values are key values in calculating for most failure criteria and inelastic part of stress.

$$\sigma_{eff.} = \frac{1}{\sqrt{2}} \sqrt{\sigma_{rr}^2 + \sigma_{zz}^2 + \sigma_{\theta\theta}^2 + 3 \sigma_{rz}^2 - \sigma_{rr}\sigma_{\theta\theta} - \sigma_{rr}\sigma_{zz}} \quad (5.2)$$

### 5.2.1.1 Forward Loaded Plate

As mentioned before, plate is divided into 4, 8 and 16 layers and results are compared with FGM plate. Volume fraction of ceramic phase is given in Figure A.22. Layers are numbered from the bottom of the plate through the top of the plate. Since the problem is one dimensional at the center of the plate, points away from the center is analyzed for the comparison FGMs and layered material. Since most of the failure criteria are function of effective stress, effective stress is compared in the first part. Derivative of effective stress is compared with respect to stresses.

Variation of effective stress in time is shown in Figure A.23 for different locations along the radius. It is seen that effective stress decreases towards the clamped end of the plate. As is seen from the figure, as the number of layers increases the results obtained from the layered medias are getting closer to the results obtained from the FGM plate.

In Figure A.24 variation of the effective stress is shown along the radius at the  $z/h = 0.375$ . Results obtained from the layered medias are very close to the results obtained from the FGM plate. On the other hand as the time proceeds very small difference occurs in between.

It is observed that as the stress wave approaches to the bottom of the plate, value of the effective stress decreases for both FGM and layered plates in Figure A.25. In addition the difference between the FGM plate and layered plates increases as the time proceeds. There is a sudden rise of the effective stress is seen at the top of the plate and this sudden rise vanishes after some time. On the other hand effective stress is almost constant in time.

Effective stress values are very close for FGM plate and layered plates in the upper part of the plate as is seen from the Figure A.26. The phase difference is clearly seen at 13  $\mu\text{sec}$ . with a slight difference afterwards. On the other hand through the lower part of the plate, the values of the phase difference begin to occur at 11  $\mu\text{sec}$ . Thus the stress waves coming from the center and clamped end meet at different times on the top and bottom of the plate. Although the the general characteristics of the effective stress is similar between the FGM and

layered plates, the difference between the effective stress values in the plates are not negligible after  $11 \mu\text{sec}$ .

Variation of  $f_{rr}$  is shown in Figure A.27 at the center of the plate. It is observed that  $f_{rr}$  values are almost the same for both FGM and layered plates at the center of the plate.

In Figure A.28  $f_{rr}$  values for various locations along the radius is shown. It is observed that until the stress wave emerges to the point the difference in  $f_{rr}$  between FGM and layered plates are significantly big. On the other hand after the stress wave arrives difference in  $f_{rr}$  between FGM and layered plates decreases.

In Figure A.29  $f_{zz}$  is shown at the center of the plate. Similar to  $f_{rr}$  values the results are very close in between results obtained from FGM plate and layered plates.

Variation of  $f_{zz}$  values at  $z/h = 0.5$  at various locations in Figure A.30. It is seen that at  $r/R = 0$ ,  $f_{zz}$  values are very close both for FGM plate and layered plates. It is observed that results begin to differ significantly toward the clamped end of the plate. In addition, as the number of layers increases difference between the results obtained from the layered plate and the results obtained from the FGM plate decreases.

$f_{rz}$  values are shown in Figure A.31. It is seen that  $f_{rz}$  values does not differ for FGM plate and layered plate. Thus shear stress does not have any effect at the center of the plate.

In Figure A.32  $f_{rz}$  values at  $z/h = 0.5$  for various locations along the radius are shown. It is seen that the values obtained from FGM plate analysis differs from values obtained from analysis of layered plates. This difference is not negligible toward the clamped end of the plate. On the other hand as the number of layers increases, the values obtained from layered plate becomes closer to the values obtained from layered plate.

Shear stress in the plate is shown in the plate in Figure A.33 at  $t = 5 \mu\text{sec}$ . and  $t = 10 \mu\text{sec}$ . It is seen from the Figure that the stress wave propagates almost with the same speed both in FGM plate and layered plates. It is seen that there

are some high frequency oscillations at the bottom of the plate. Also it is observed that this high frequency oscillations does not propagate through the rest of the plate. Therefore one can conclude that these high frequency errors are due to the numerical error.

#### **5.2.1.2 Backward Loaded Plate**

Similar to the forward loaded plate, backward loaded plate is divided into 4, 8 and 16 layers and results are compared with FGM plate. Volume fraction of ceramic phase is given in Figure A.34.

Variation of effective stress in time is shown in Figure A.35 for different locations along the radius. It is seen that effective stress decreases towards the clamped end of the plate. As is seen from the figure, as the number of layers increases the results obtained from the layered medias are getting closer to the results obtained from the FGM plate. In addition one can say that stress wave propagates faster in FGM plate than layered plates. Thus the upper part of the FGM plate is stiffer than layered plates.

In Figure A.36 variation of the effective stress is shown along the radius at the  $z/h = 0.375$ . It is observed that some of the extremum points, which are seen in 8, 16 layered and FGM plate, are not seen in 4 Layered plates. In addition as the number of layers increases results are getting closer to the FGM plate.

In Figure A.37, effective stress values at  $r/R = 0.2$  is shown. There is approximately %10 difference between 4 Layered plate and FGm plate. The difference decreases as the number of layers increases. There is a sudden rise of the effective stress is seen and this sudden rise vanishes after some time. In addition effective stress is almost constant in time. It is observed that the magnitude of the effective stress does not change significantly through the bottom of the plate. One can say that stress wave propagates faster in FGM plate on the top, whilst it propagates slower than layered plates at the lower parts of the plates.

Effective stress values are significantly different for FGM plate and layered plates at the far end of the plate as is seen from the Figure A.38. Stress wave in FGM plate propagates more faster in FGM plate than layered plates.

It is observed that  $f_{rr}$  values are different for FGM and layered plates at the upper part of the plate in Figure A.39. The values are getting closer through the bottom of the plate as the volume fractions of the material phases are getting closer.

In Figure A.40  $f_{rr}$  values for various locations along the radius is shown. It is seen that  $f_{rr}$  values differs significantly through the clamped end of the plate. In addition difference is negligible at the center of the plate.

In Figure A.41 is shown at the center of the plate. Similar to  $f_{rr}$  values the results are very close in between results obtained from FGM plate and layered plates at the bottom of the plate. Results are different at the top plate. Thus the volume fractions of the material phases are different.

Variation of  $f_{zz}$  values at  $z/h = 0.5$  at various locations along the radius is shown in Figure A.42. It is seen that at  $r/R = 0.$ , difference in  $f_{zz}$  values between FGM plate and layered plate are very close. It is observed that results begin to differ significantly through the clamped end of the plate. In addition, as the number of layers increases difference between the results obtained from the layered plate and the results obtained from the FGM plate decreases. It is also seen that results obtained from 4 Layered plate is more oscillatory.

In Figure A.43  $f_{rz}$  values at  $z/h = 0.5$  for various locations along the radius are shown. It is seen that the values obtained from FGM plate analysis differs from values obtained from analysis of layered plates. This difference is not negligible through the clamped end of the plate. In addition there are some extremum points observed in 4 Layered plate. These peaks vanishes through the clamped end as the time proceeds.

Shear stress in the plate is shown in Figure A.44 at  $t = 5 \mu sec.$  and  $t = 10 \mu sec.$ . It is seen from the Figure that the stress wave propagates faster in FGM plate than layered plates. In addition wave front is more uniform in FGM than layered plates. It is seen that there are some high frequency oscillations at the bottom of the plate. Similar to the forward loaded plate, there are high frequency oscillations observed at the bottom of the plate.



## 6. CONCLUSIONS AND FUTURE WORK

Conservation properties are investigated by using shockwave propagation problem for long time computations. In this study, it is observed that small time steps in TDG may lead to divergence of the solution. To overcome this difficulty coarse mesh reproduced in space and stable solutions are obtained. It is observed that dissipation is very small compared to other methods. Therefore one can conclude that TDG is suitable for long time interval analysis as is seen in the shockwave propagation problem.

Bar impact on a rigid wall problem is solved by using the proposed formulation. The effect of element size and time step is studied. It is observed that time step is the main parameter that controls the accuracy of the numerical solution. Since all the waves, which have lower period than the time step are damped [?], the selection of the time step is the critical issue. Small time steps may cause divergence of the numerical solution. One can say that time step should be selected such that CFL number is around 1. Therefore time step has to be chosen according to the physical wave that is of interest. By doing this, high resolution numerical solutions can be obtained without using artificial dissipation terms in shock wave propagation problems. It is also observed that decay in energy is very low in space-time formulation.

Bi-material rigid bar impacting on a rigid wall problem is also studied. The considerations on the choice of time steps as in the first problem are observed. The effect of power of the trial polynomials is investigated. It is determined that as the order of polynomial increases, resolution of the numerical solutions increases. On the other hand, it may lead to divergence in some cases. Added stabilization terms affect and improve the accuracy, convergency and conservation property of the proposed space-time formulation. Also sudden changes in material properties cause dispersion in the solution which is not damped when the small

time steps are used. Dispersion leads to divergence in some cases. It is also determined that there is a small increase in the total energy with the increase in element size.

In the  $1D$  analysis of FGMs and layered media, it is observed using small time steps may lead to divergence because of the dispersion caused by sudden change in stress at a point both for FGM and layered media. In addition sudden changes in material properties cause dispersion in the solution which is not damped when small time steps are used. Dispersion leads to divergence in some cases. Similar to the  $1D$  problems CFL shall be around 1 to have an accurate solution for two dimensional problems. It is seen that using linear variation of material properties along with discontinuous Galerkin method is successful in modelling the mechanical behavior of FGMs. In addition mechanical behavior of FGM and layered media is very similar for one dimensional problems apart from small oscillations in layered media caused by the sudden changes in material properties. It is also seen that peak stresses are higher in FGM than in layered media.

Two dimensional axis-symmetric layered plate is studied as a two dimensional test case. In this case, high frequency oscillations are damped. Therefore numerical solution converges for most time steps and element sizes. The numerical oscillations, caused by the large impedance change between the layers, do not affect the overall solution, since they do not propagate to the rest of the domain. Therefore, it may be concluded that space-time discontinuous Galerkin formulation proposed in this study is also successful in modelling two dimensional problems.

The proposed space-time discontinuous Galerkin formulation is very robust and successful in modelling shock wave propagation. Even though there are some disadvantages, (i.e., high computational cost) space-time discontinuous Galerkin method is found to be accurate in modelling solid dynamics problems.

## REFERENCES

- [1] **Jones, R.M.**, 1998. Mechanics of Composite Materials, Ann Arbor, MI., Taylor & Francis Inc.
- [2] **Chung, P.W., Tamma, K.K. and Namburu, R.R.**, 2001. Asymptotic expansion homogenization for heterogeneous media: computational issues and applications, *Composites Part A: Applied Science and Manufacturing*, **32**, 1291–1301.
- [3] **Hori, M. and Nemat-Nasser, S.**, 1999. Theories for Determining Micro-Macro Relations in Heterogeneous Solids, *Mechanics of Materials*, **31**, 667–682.
- [4] **Belytscko, T., Liu, W.K. and Moran, B.**, 2000. Nonlinear Finite Elements for Continua and Structures, Chichester ; New York, Willey.
- [5] **Achenbach, J.D.**, 1973. Wave Propagation in Elastic Solids, Amsterdam, North-Holland Publishing Company.
- [6] **Sun, C.T., Achenbach, J.D. and Herrmann, G.**, 1968. Continuum Theory for a Laminated Medium, *Journal of Applied Mechanics*, **35**, 467–473.
- [7] **Lundergan, C.D. and Drumheller, D.S.**, 1971. ropagation of Stress Waves in Laminated Plate Composite, *Journal of Applied Physics*, **42**, 669–675.
- [8] **Chen, X., Chandra, N. and Rajendran, A.**, 2004. Analytical Solution to the Plate Impact Problem of Layered Heterogeneous Material Systems, *International Journal of Solids and Structures*, **41**, 4635–4659.
- [9] **Li, Y., Ramesh, K.T. and Chin, E.S.C.**, 2001. Dynamic Characterization of Layered and Graded Structures Under Impulsive Loading, *International Journal of Solids and Structures*, **38**, 6045–6061.
- [10] **Lee, E.H., Budiansky., B. and Drucker, D.C.**, 1975. On The Influence of Variations of Material Properties on Stress Wave Propagation Through Elastic Slabs, *Journal of Applied Mechanics*, **42(2)**, 417–422.
- [11] **Santare, M.H., Thamburaj, P. and Gazonas, G.A.**, 2003. The Use of Graded Finite Elements in the Study of Elastic Wave Propagation

in Continuously Nonhomogeneous Materials, *International Journal of Solids and Structures*, **40**, 5621–5634.

- [12] **Banks-Sills, L., Eliasi, R. and Berlin, Y.**, 2002. Modelling of Functionally Graded Materials in Dynamic Analyses, *Composites Part B: engineering*, **33**, 7–15.
- [13] **Berezovski, A., Engelbrech, J. and Maugin, G.A.**, 2003. Numerical Solution of Two Dimensional Wave Propagation in Functionally Graded Materials, *European Journal Mechanics*, **22**, 257–265.
- [14] **El-Raheb, M. and Tham, R.**, 1997. Transient Waves in a Periodic Stack: Experiments and Comparison with Analysis, *Journal of Acoustical Society of America*, **101**, 860–866.
- [15] **Newmark, N.M.**, 1959. A Method of Computation for Structural Dynamics, *Journal of the Engineering Mechanics Division ASCE*, **8**, 67–94.
- [16] **Kane, C., Marsden, J.E., Ortiz, M. and West, M.**, 2000. Variational Integrators and the Newmark Algorithm for Conservative and Dissipative Mechanical Systems, *International Journal For Numerical Methods in Engineering*, **49**, 1295–1325.
- [17] **Simo, J.C., Tarnow, N. and Wong, K.K.**, 1992. Exact Energy-Momentum Conserving Algorithms and Symplectic Schemes for Nonlinear Dynamics, *Computer Methods in Applied Mechanics and Engineering*, **100**, 63–116.
- [18] **Bauchau, O.A. and Joo, T.**, 1999. Computational Schemes for Non-Linear Elasto-Dynamics, *International Journal For Numerical Methods in Engineering*, **45**, 693–719.
- [19] **Cella, A., Lucchesi, M. and Pasquinelli, G.**, 1980. Space-Time Elements for the Shock Wave Propagation Problem, *International Journal For Numerical Methods in Engineering*, **15**, 1475–1488.
- [20] **Betsch, P. and Steinmann, P.**, 2001. Conservation Properties of a Time FE Method Part II: Time-Stepping Schemes for Non-Linear Elastodynamics, *International Journal For Numerical Methods in Engineering*, **50**, 1931–1955.
- [21] **Lesaint, P. and Raviart, P.A.**, 1974. in *Mathematical Aspects of Finite Elements in Partial Differential Equations*, ed. C. de Boor, chapter On a Finite Element Method for Solving the Neutron Transport Equation, Academic Press: New York, pp. 89–145.
- [22] **Hughes, T.J.R. and Hulbert, G.M.**, 1988. Space-Time Finite Element Methods for Elastodynamics: Formulations and Error Estimates, *Computer Methods in Applied Mechanics and Engineering*, **66**, 339–363.

- [23] **Chien, C.C., Yang, C.S. and Tang, J.H.**, 2003. Three-Dimensional Transient Elastodynamics Analysis by a Space and Time-Discontinuous Galerkin Finite Element Method, *Finite Elements in Analysis and Design*, **39**, 561–580.
- [24] **Bonelli, A. and Bursi, O.S.**, 2003. Iterative Solutions for Implicit Time Discontinuous Galerkin Methods Applied to Non-Linear Elastodynamics, *Computational Mechanics*, **30**, 487–498.
- [25] **Li, X.D. and Wiberg, N.E.**, 1998. Implementation and Adaptivity of A Space-Time Finite Element Method for Structural Dynamics, *Computer Methods in Applied Mechanics and Engineering*, **156**, 211–229.
- [26] **Kanapady, R. and Tamma, K.K.**, 2003. On a novel design of a new unified variational framework of discontinuous/continuous time operators of high order and equivalence, *Finite Elements in Analysis and Design*, **39**, 727–749.
- [27] **Pian, T.H.H.**, 1976. Variational Principles for Incremental Finite Element Methods, *Journal of the Franklin Institute*, **302**, 473–488.
- [28] **Wellford, L.C. and Oden, J.**, 1976. A Theory of Discontinuous Finite Element Galerkin Approximation of Shock Waves in Nonlinear Elastic Solids Part2:Accuracy and Convergence, *Computer Methods in Applied Mechanics and Engineering*, **8**, 17–36.
- [29] **Huang, H. and Costanzo, F.**, 2002. On the Use of Space-Time Finite Elements in the Solution of Elasto-Dynamic Problems with Strain Discontinuities, *Computer Methods in Applied Mechanics and Engineering*, **191**, 5315–5343.
- [30] **Aksoy, H.G., Tanriover, H. and Senocak, E.**, 2004, Houston-Texas, USA. Comparison of Newmark and Space-Time Discontinuous Galerkin Method, **R.B. Malla and A. Maji**, editors, in *Proceedings of Earth&Space 2004: Engineering, Construction, and Operations in Challenging Environments*, pp. 532–539.
- [31] **Palaniappan, J., Haber, R.B. and Jerrard, R.L.**, 2004. A Spacetime Discontinuous Galerkin Method for Scalar Conservation Laws, *Computer Methods in Applied Mechanics and Engineering*.
- [32] **Lowrie, R.B.**, 1996. Compact Higher-Order Numerical Methods For Hyperbolic Conservation Laws, Ph.D. thesis, University of Michigan Ann Arbor, Michigan, USA.
- [33] **Baumann, C.E.**, 1997. An HP-Adaptive Discontinuous Finite Element Method For Computational Fluid Dynamics, Ph.D. thesis, University of Texas at Austin, Texas, USA.
- [34] **Cockburn, B. and Shu, C.W.**, 1998. The Local Discontinuous-Galerkin Method for the Time-Dependent Convection-Diffusion Systems, *SIAM Journal on Numerical Analysis*, **35(6)**, 2440–2463.

- [35] **Zhang, M. and Shu, C.W.**, 2003. An Analysis of Three Different Formulations of the Discontinuous Galerkin Method For Diffusion Equations, *Mathematical Models and Methods in Applied Sciences*, **13(3)**, 395–413.
- [36] **Zienkiewicz, O.C., Taylor, R.L., Sherwin, S.J. and Peiro, J.**, 2003. On Discontinuous Galerkin Methods, *International Journal For Numerical Methods in Engineering*, **58**, 1119–1148.
- [37] **Aksoy, H.G. and Senocak, E.**, 2008. Space-Time Discontinuous Galerkin Method for Dynamics of Solids, *Communications in Numerical Methods in Engineering*, (in press).
- [38] **Chiu, T.C. and Erdogan, F.**, 1999. One-Dimensional Wave Propagation in a Functionally Graded Elastic Medium, *Journal of Sound and Vibration*, **222**, 453–487.
- [39] **Eringen, A.C. and Suhubi, E.S.**, 1974. Elastodynamics Vol. 1, New York, NY., Academic Press.
- [40] **Thomas, T.Y.**, 1961. Plastic Flow and Fracture in Solids, New York and London, Academic Press.
- [41] **Oden, J., Babuška, I. and Baumann, C.**, 1998. A Discontinuous hp Finite Element Method for Diffusion Problems, *Journal of Computational Physics*, **146**, 491–519.
- [42] **Hansbo, P. and Larson, M.G.**, 2002. Discontinuous Galerkin Methods for Incompressible and Nearly Incompressible Elasticity by Nitsche's Method, *Computer methods in applied mechanics and engineering*, **191**, 1895–1908.
- [43] **Hughes, T.**, 1983. in Computational Methods For Transient Analysis, ed. T. Belytschko and T.J.R. Hughes, chapter Analysis of Transient Algorithms with Particular Reference to Stability, Elsevier Science Publishing Company Inc., pp. 67–155.

## A. Figures

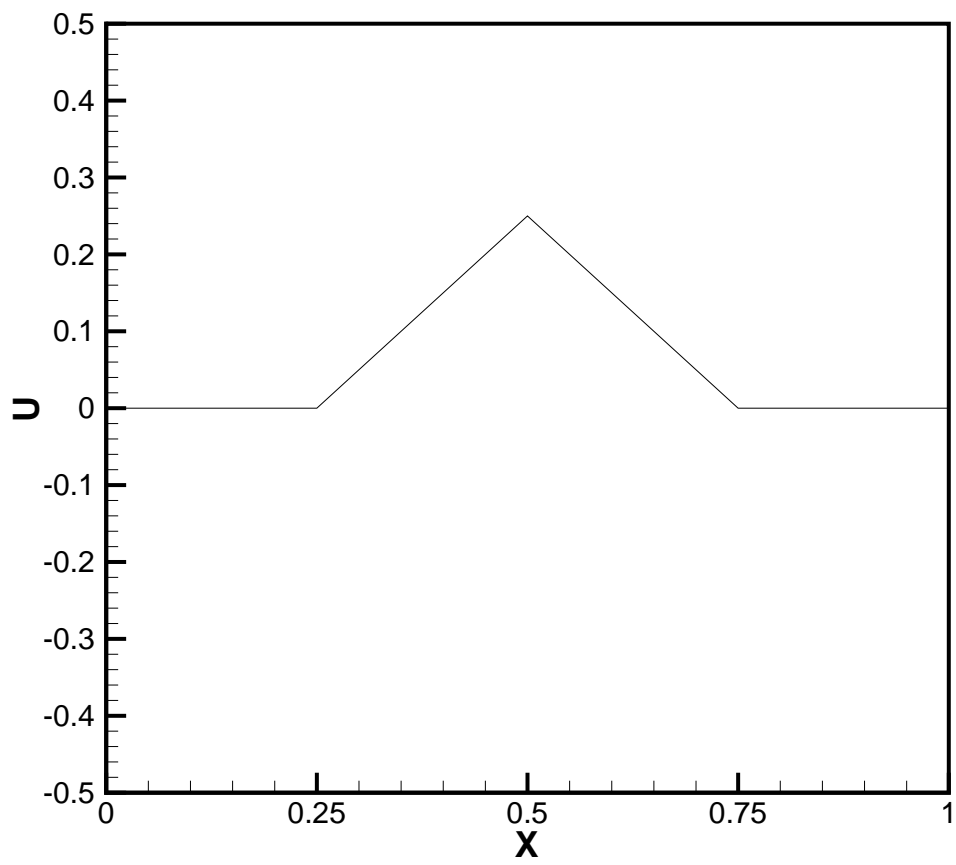
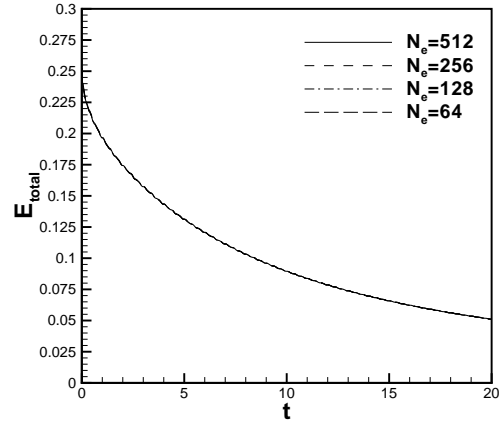
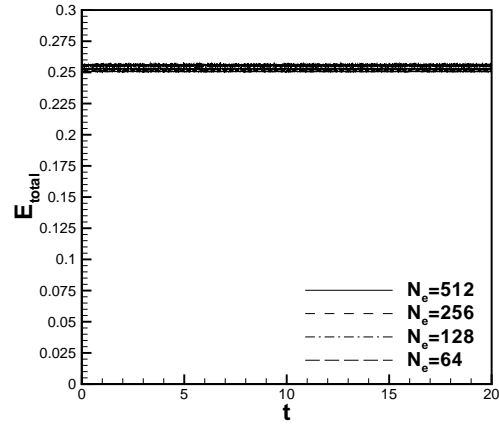


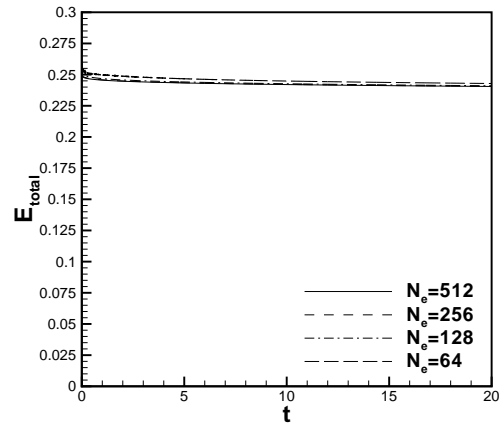
**Figure A.1:** Initial displacement field for shock wave propagation problem.



(a) Newmark with  $\beta = 0.5, \gamma = 1.0$



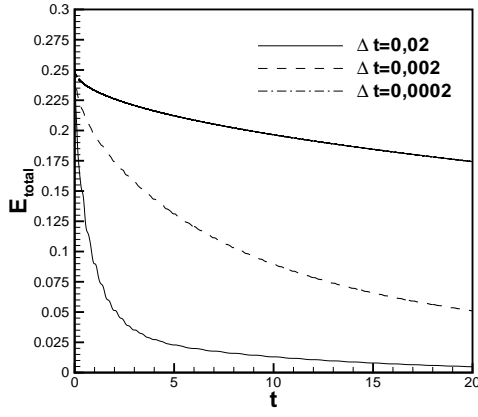
(b) Newmark with  $\beta = 0.25, \gamma = 0.5$



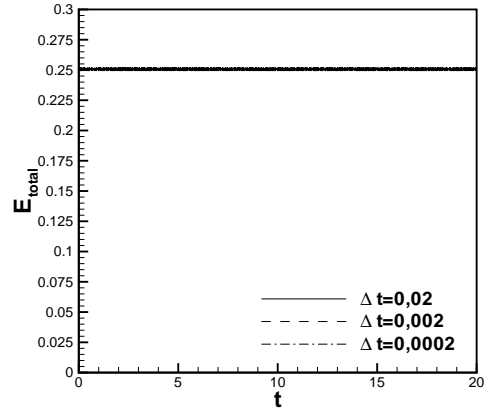
(c) Time Discontinuous Galerkin

**Figure A.2:** Conservation of energy for different mesh sizes ( $\Delta t = 0.002$ ).

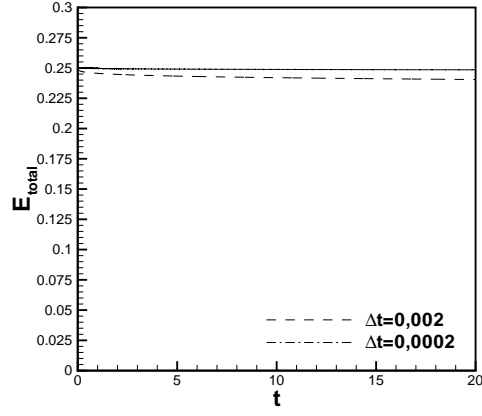




(a) Newmark with  $\beta = 0.5, \gamma = 1.0$

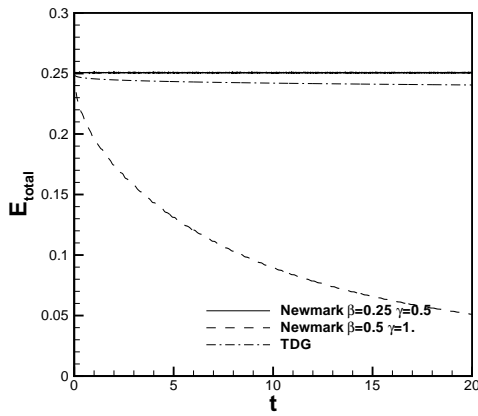


(b) Newmark with  $\beta = 0.25, \gamma = 0.5$

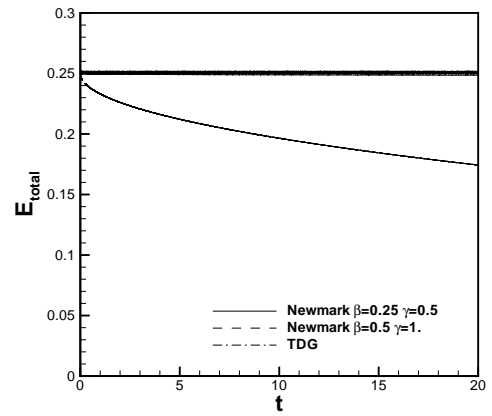


(c) Time Discontinuous Galerkin

**Figure A.3:** Variation of total energy for different time steps ( $N_e = 512$ ).

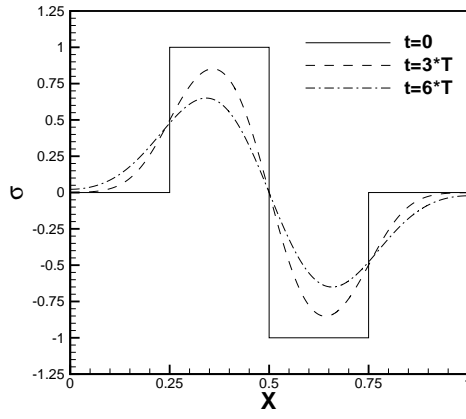


(a)  $\Delta t = 0.002$

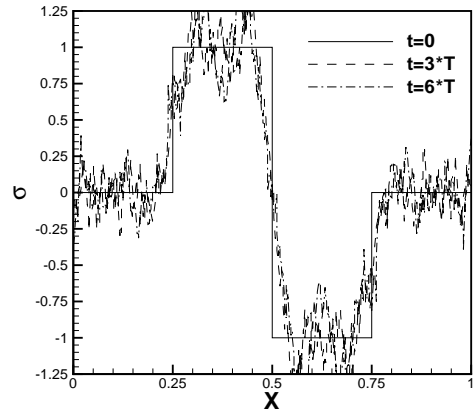


(b)  $\Delta t = 0.0002$

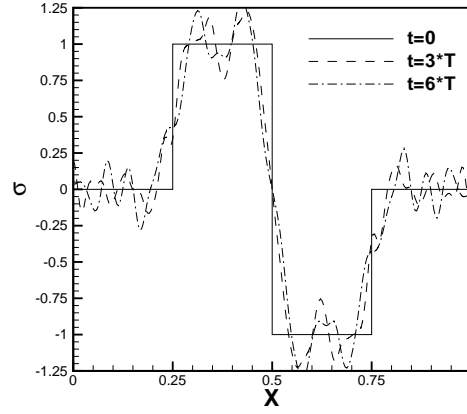
**Figure A.4:** Comparison of Newmark method and TDG for different time steps ( $N_e = 512$ ).



(a) Newmark with  $\beta = 0.5, \gamma = 1.0$



(b) Newmark with  $\beta = 0.25, \gamma = 0.5$



(c) Time Discontinuous Galerkin

**Figure A.5:** Stress at 3<sup>rd</sup> and 6<sup>th</sup> periods for different methods.

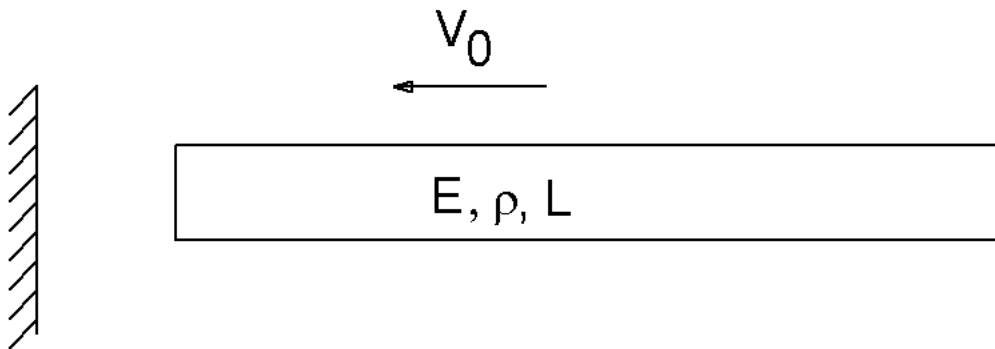
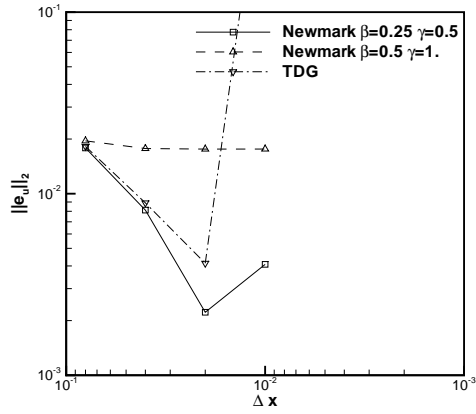
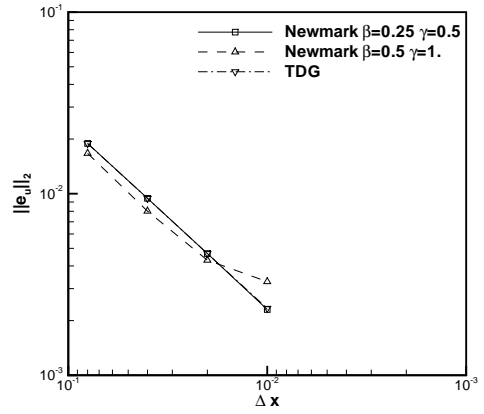


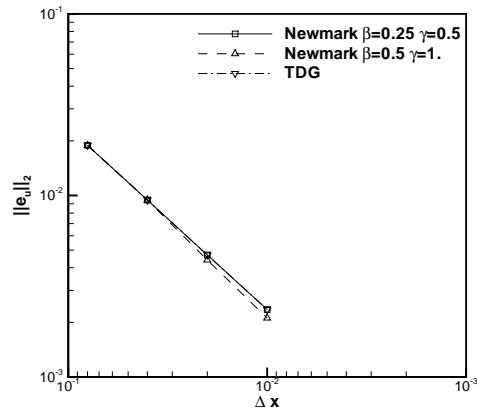
**Figure A.6:** Bar impact on a rigid wall problem.



(a)  $\Delta t = 0.02$

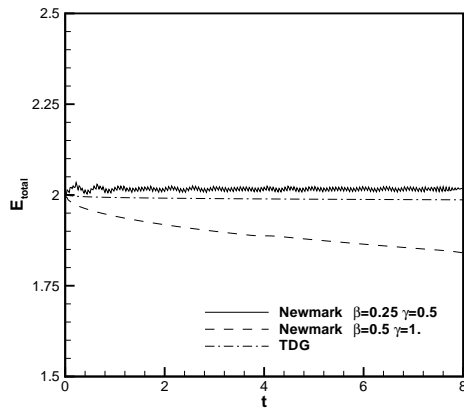


(b)  $\Delta t = 0.002$

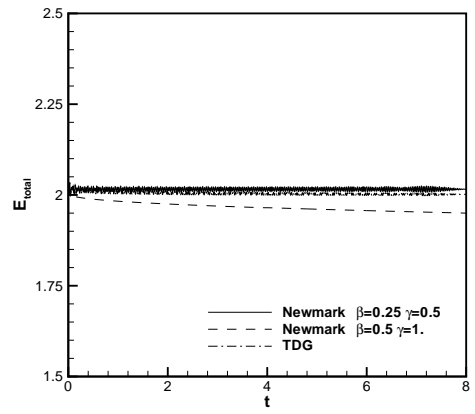


(c)  $\Delta t = 0.0002$

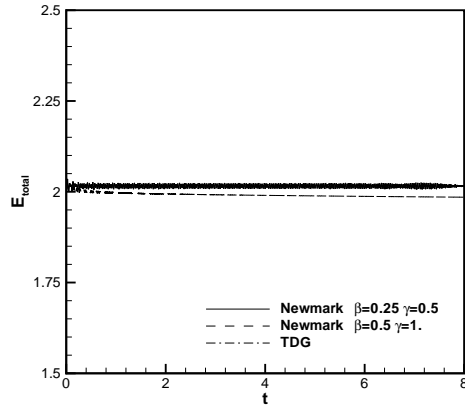
**Figure A.7:**  $L_2$  norm of the error in displacement at different time steps at  $t = 2$  for bar impact problem.



(a)  $\Delta t = 0.02$

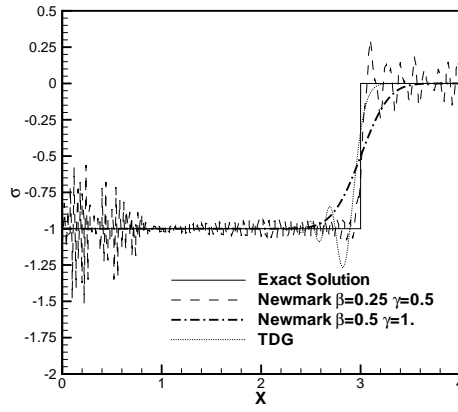


(b)  $\Delta t = 0.002$

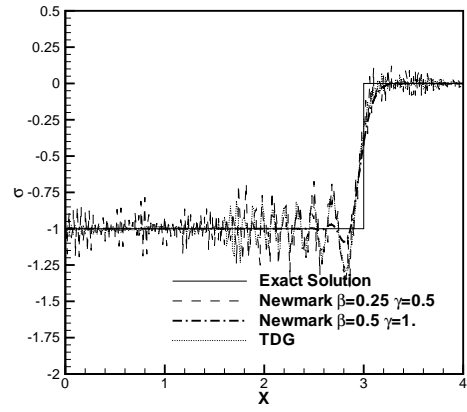


(c)  $\Delta t = 0.0002$

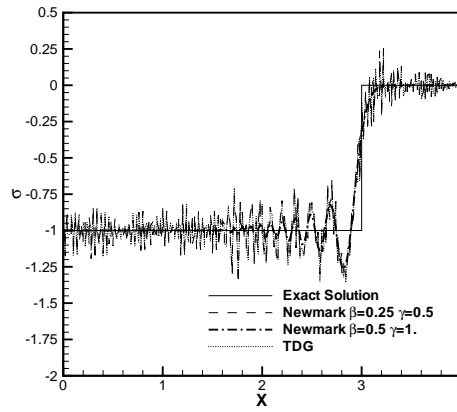
**Figure A.8:** Total energy variation at different time steps for bar impact problem.



(a)  $\Delta t = 0.02$



(b)  $\Delta t = 0.002$



(c)  $\Delta t = 0.0002$

**Figure A.9:** Comparison of the stress in the bar at  $t = 5$  for bar impact problem.

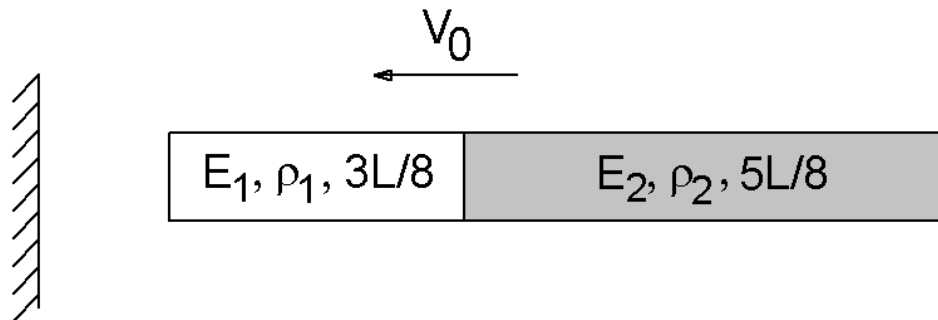
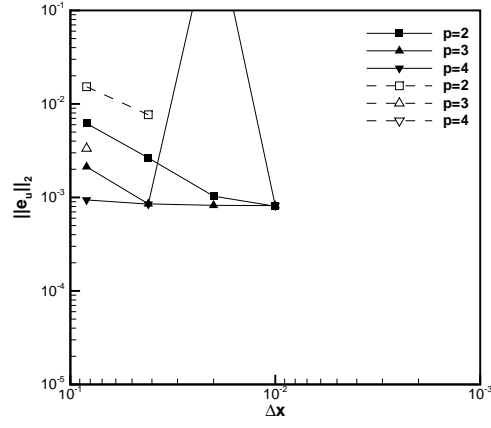
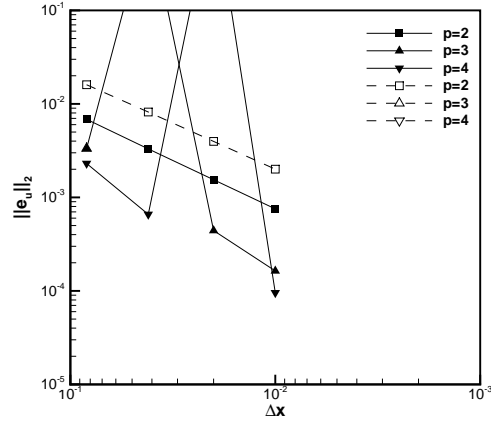


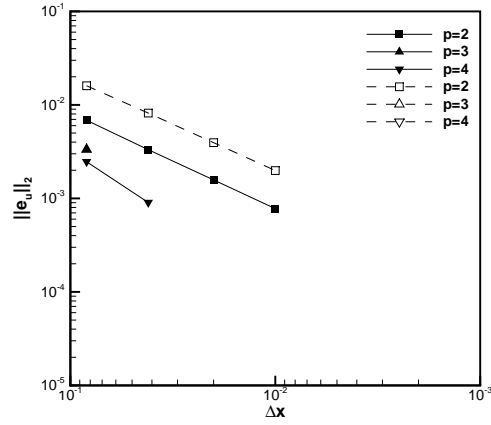
**Figure A.10:** Bi-material bar impact on a rigid wall problem.



(a)  $\Delta t = 0.02$

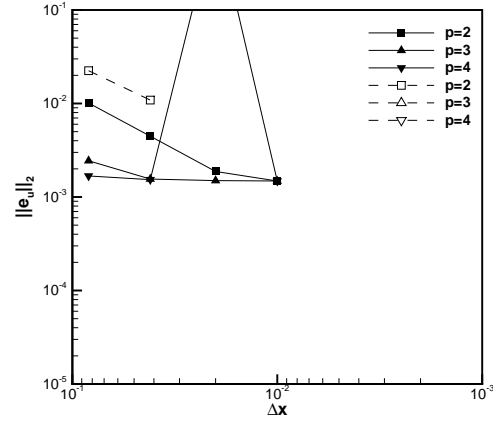


(b)  $\Delta t = 0.002$

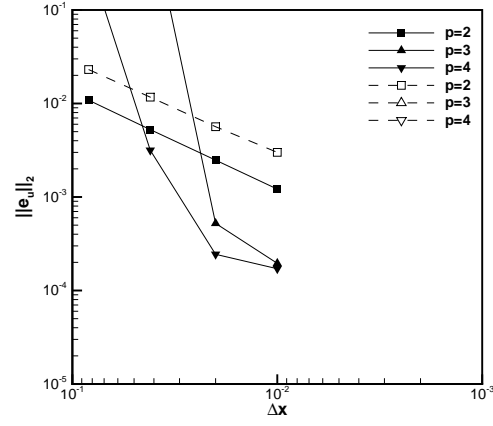


(c)  $\Delta t = 0.0002$

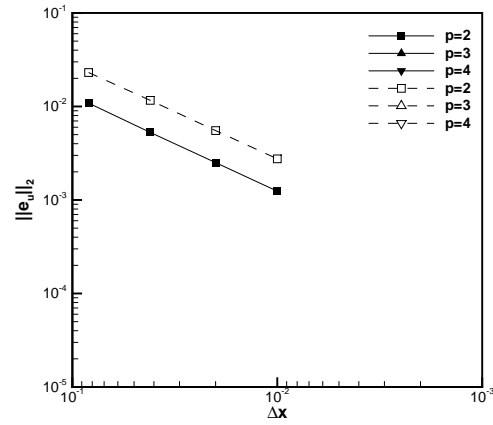
**Figure A.11:**  $L_2$  norm of the error in displacement at different time steps at  $t = 1.5$  for bi-material bar impact problem; (—: stabilized DGM, - - -: DGM).



(a)  $\Delta t = 0.02$

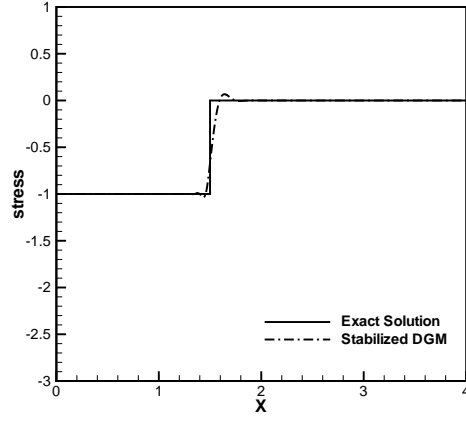


(b)  $\Delta t = 0.002$

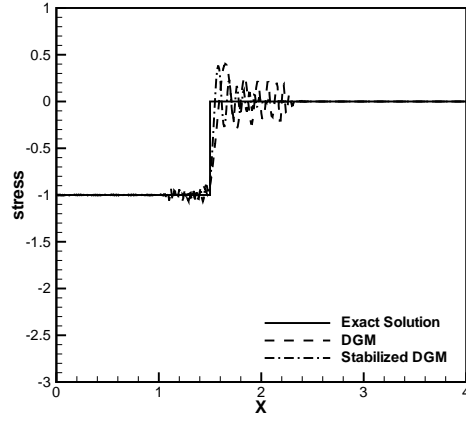


(c)  $\Delta t = 0.0002$

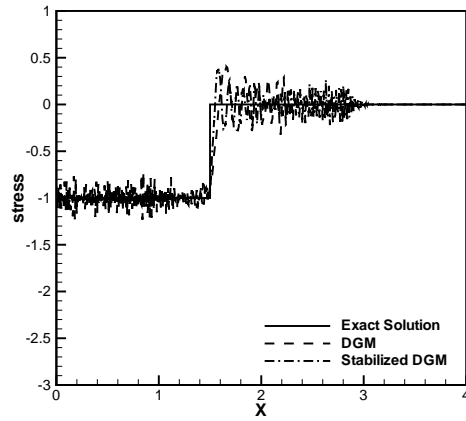
**Figure A.12:**  $L_2$  norm of the error in displacement at different time steps at  $t = 4.5$  for bi-material bar impact problem; (—: stabilized DGM, - - -: DGM).



(a)  $\Delta t = 0.02$



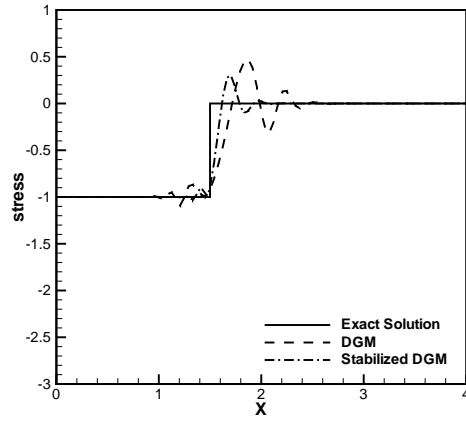
(b)  $\Delta t = 0.002$



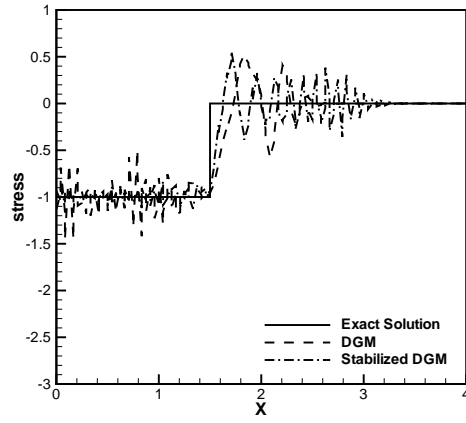
(c)  $\Delta t = 0.0002$

**Figure A.13:** Stress in the bar at  $t = 1.5$  for bi-material bar impact problem ( $N_e = 400$ ,  $p = 2$ ).

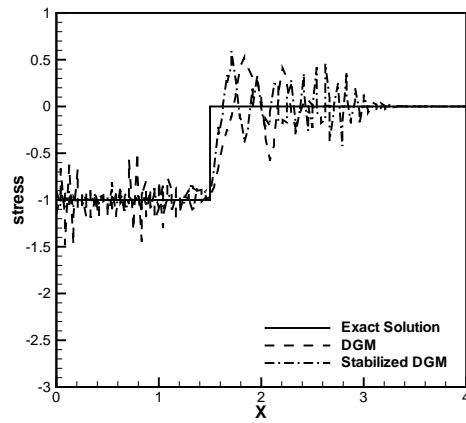




(a)  $\Delta t = 0.02$

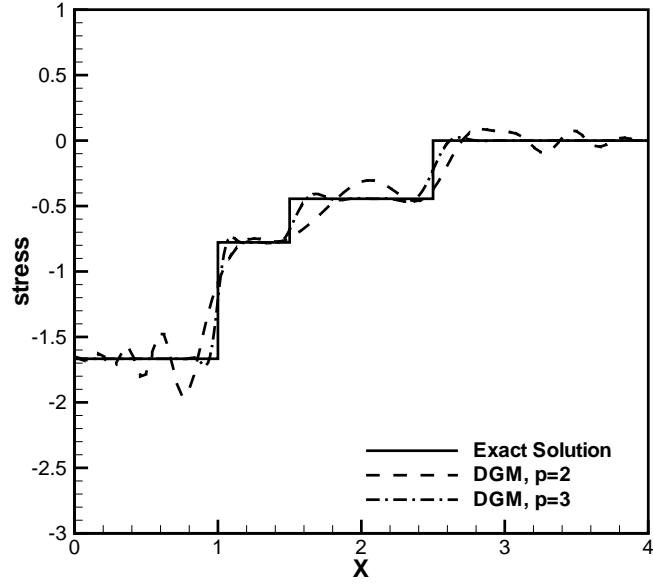


(b)  $\Delta t = 0.002$

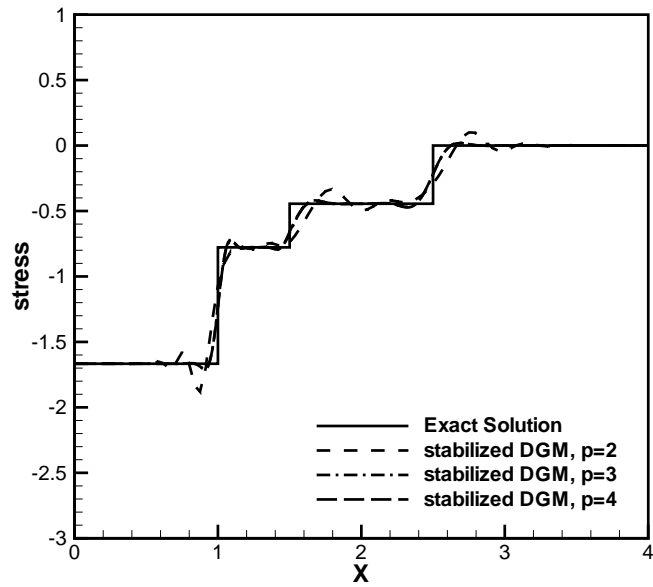


(c)  $\Delta t = 0.0002$

**Figure A.14:** Stress in the bar at  $t = 1.5$  for bi-material bar impact problem ( $N_e = 96$ ,  $p = 2$ ).



(a) DGM



(b) stabilized DGM

**Figure A.15:** Stress in the bar at  $t = 4.5$  for bi-material bar impact problem ( $N_e = 96$ ,  $\Delta t = 0.02$ ).

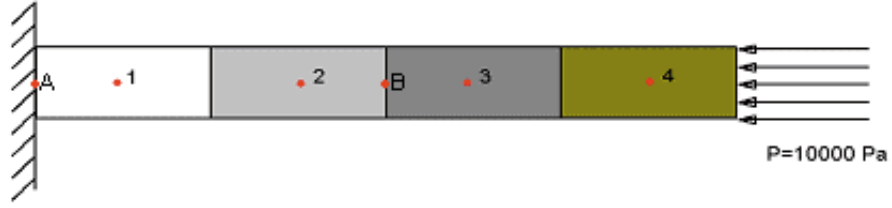
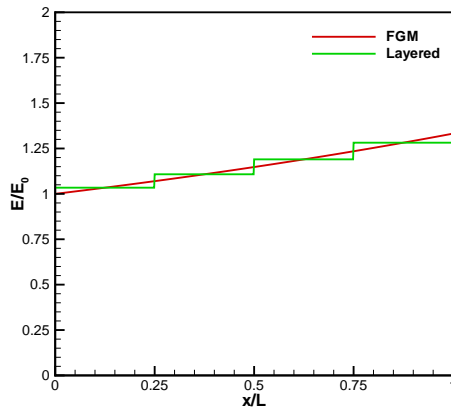
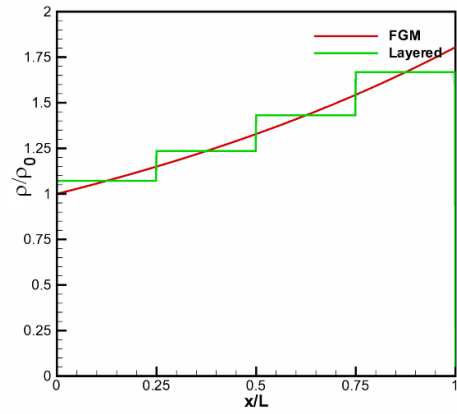


**Figure A.16:** One dimensional bar.

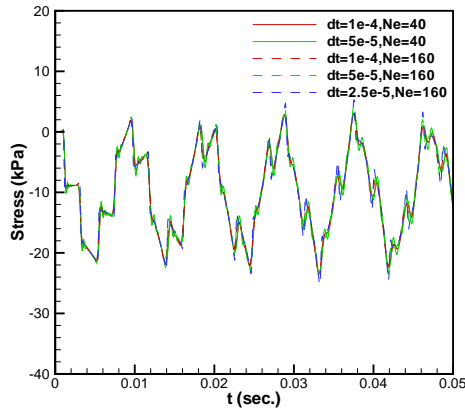


(a) Young's Modulus

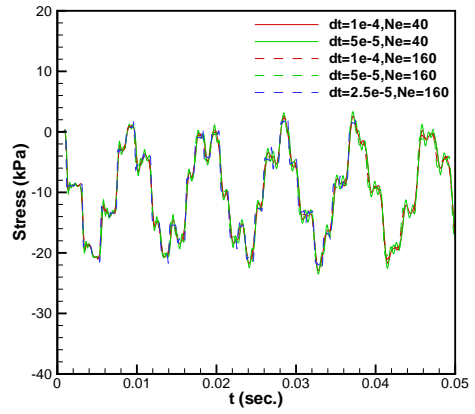


(b) Density

**Figure A.17:** Material properties along the bar.

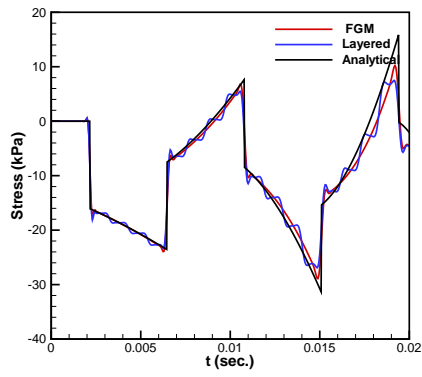


(a) FGM

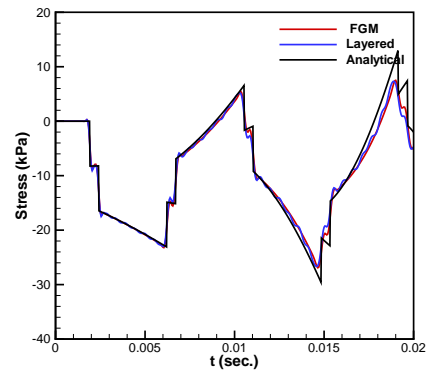


(b) Layered Bar

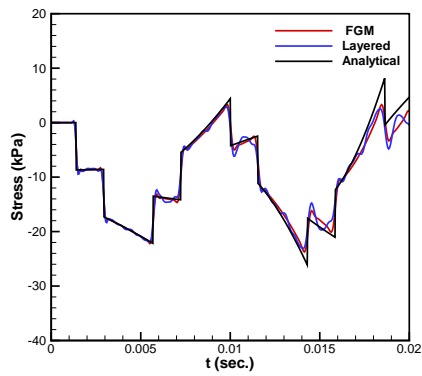
**Figure A.18:** Results of different mesh sizes and time steps at point B; —: FGM, - -: Layered.



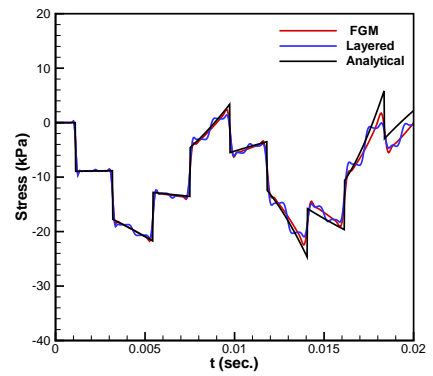
(a) Point A



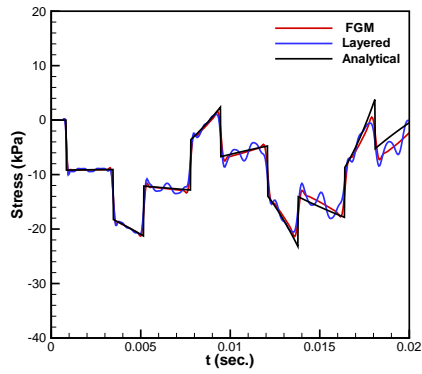
(b) Point 1



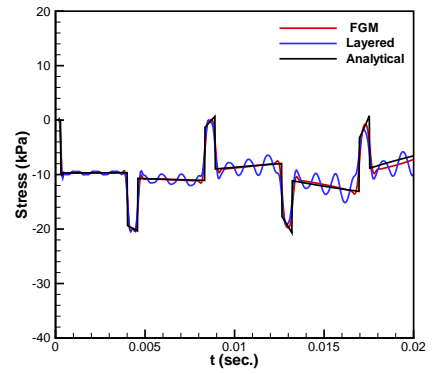
(c) Point 2



(d) Point B



(e) Point 3



(f) Point 4

**Figure A.19:** Variation of stress on the bar at different points.

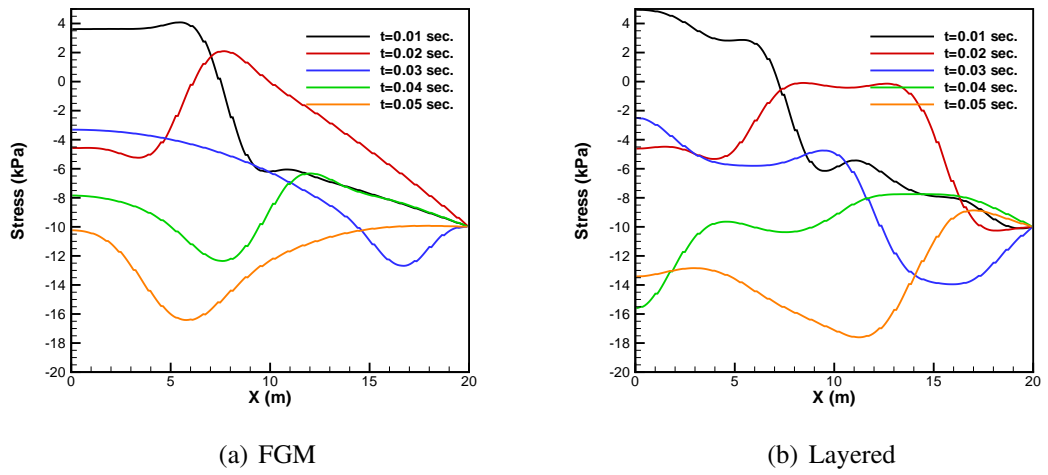


**Figure A.20:** Variation of stress along the bar at different times.

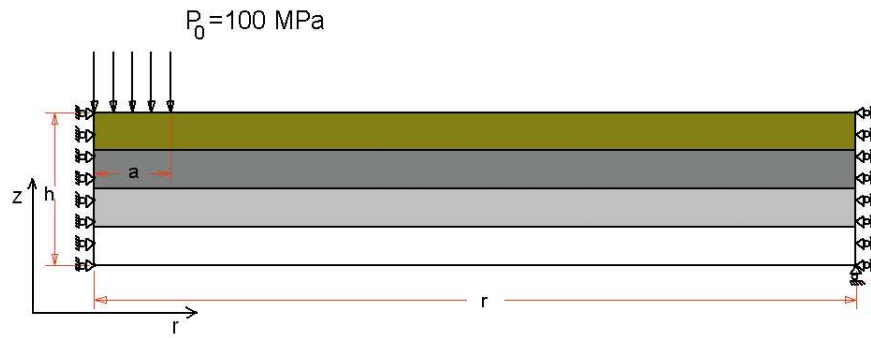


**Figure A.21:** Axi-symmetric plate loaded from its center.

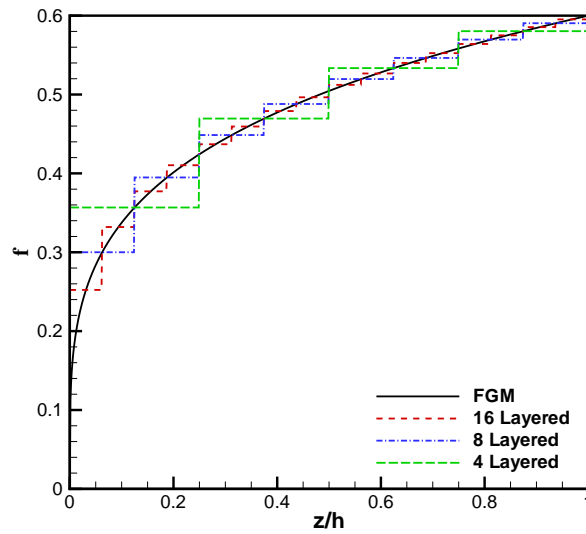
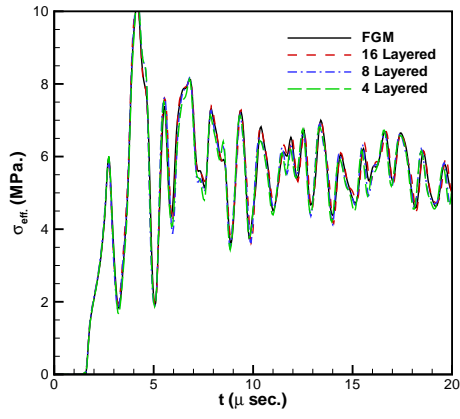
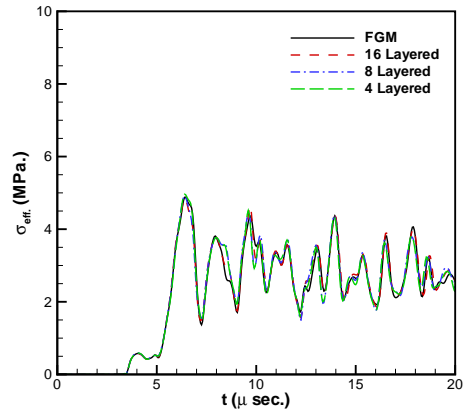


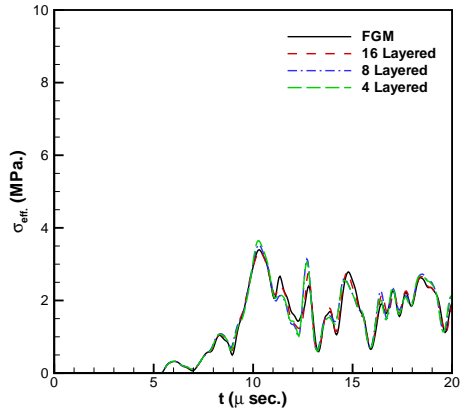
**Figure A.22:** Variation of volume fraction of ceramic phase among the thickness.



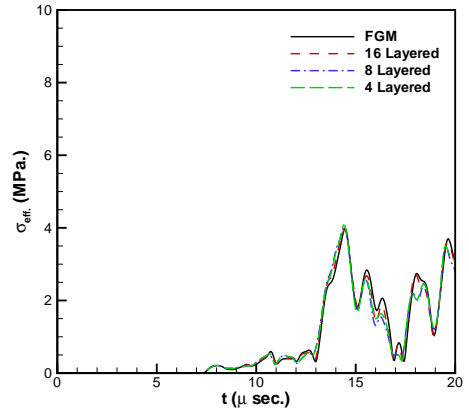
(a)  $r/R = 0.2$



(b)  $r/R = 0.4$

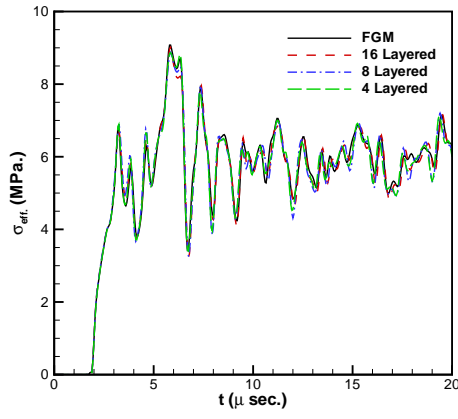


(c)  $r/R = 0.6$

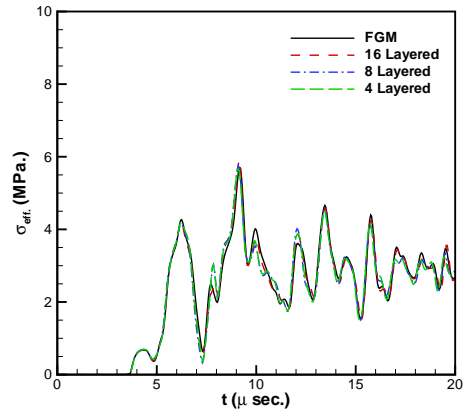


(d)  $r/R = 0.8$

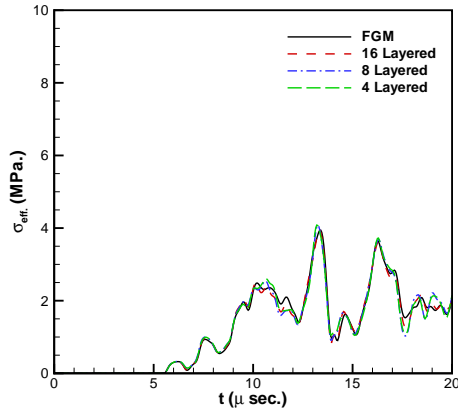
**Figure A.23:** Effective stress along the radius at  $z/h = 0.625$ .



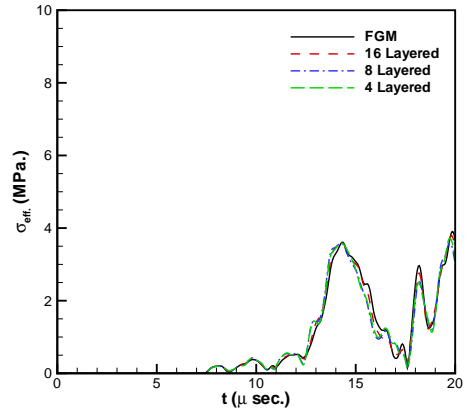
(a)  $r/R = 0.2$



(b)  $r/R = 0.4$

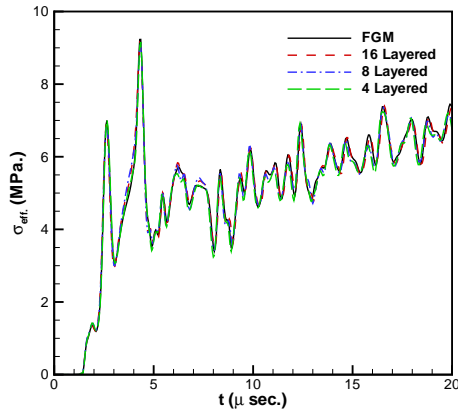


(c)  $r/R = 0.6$

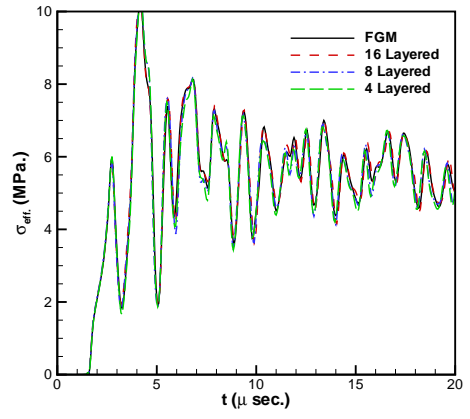


(d)  $r/R = 0.8$

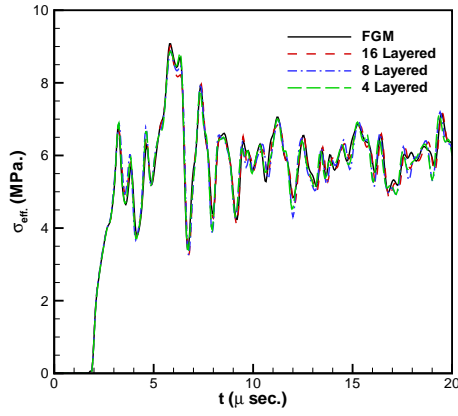
**Figure A.24:** Effective stress among the radius at  $z/h = 0.375$ .



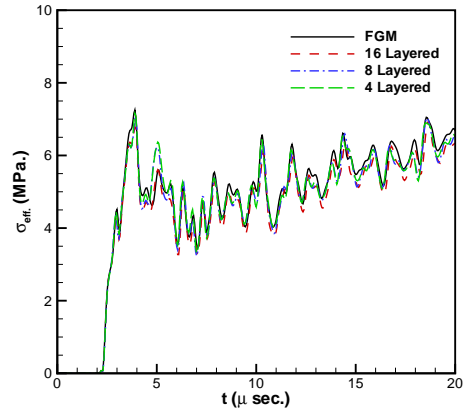
(a)  $z/h = 0.875$



(b)  $z/h = 0.625$



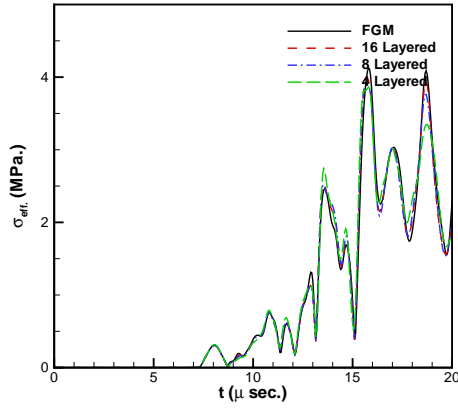
(c)  $z/h = 0.375$



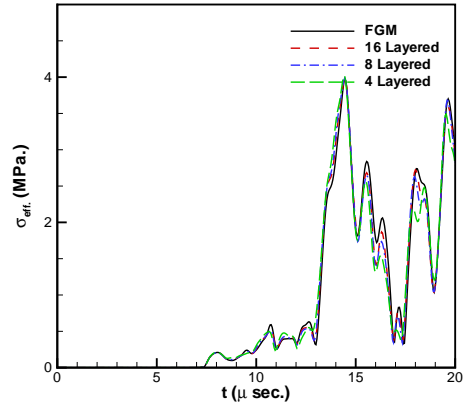
(d)  $z/h = 0.125$

**Figure A.25:** Effective stress among the thickness at  $r/R = 0.2$ .

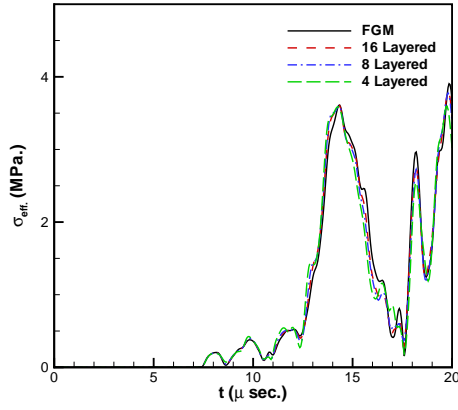




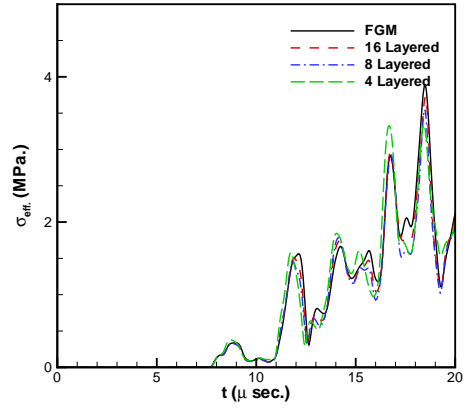
(a)  $z/h = 0.875$



(b)  $z/h = 0.625$

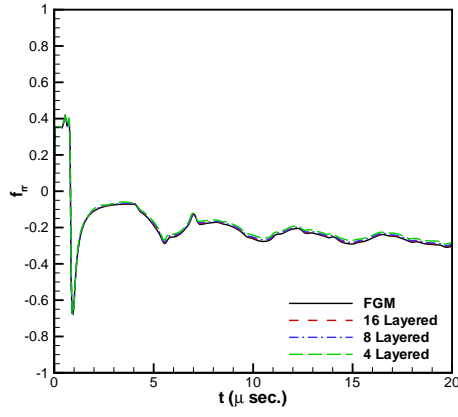


(c)  $z/h = 0.375$

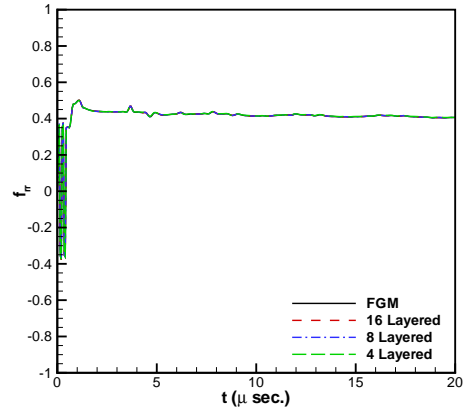


(d)  $z/h = 0.125$

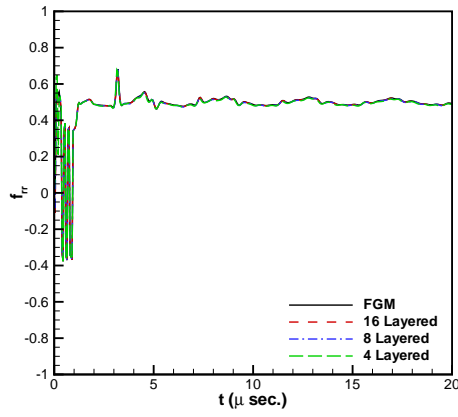
**Figure A.26:** Effective stress among the thickness at  $r/R = 0.8$ .



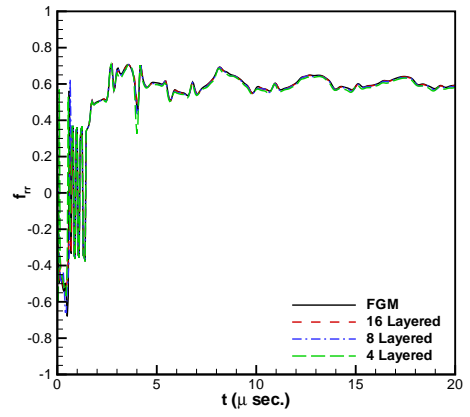
(a)  $z/h = 1.0$



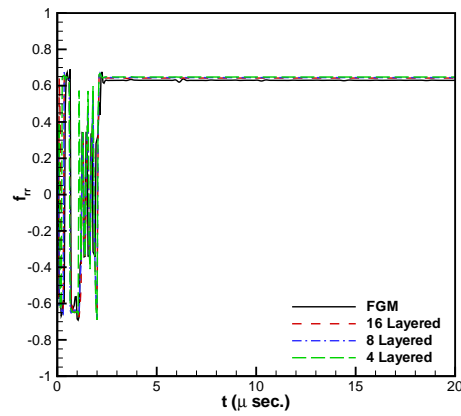
(b)  $z/h = 0.75$



(c)  $z/h = 0.5$

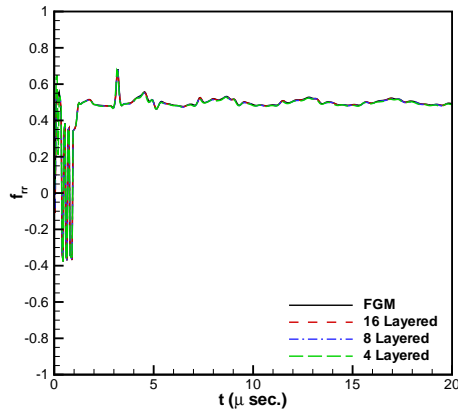


(d)  $z/h = 0.25$

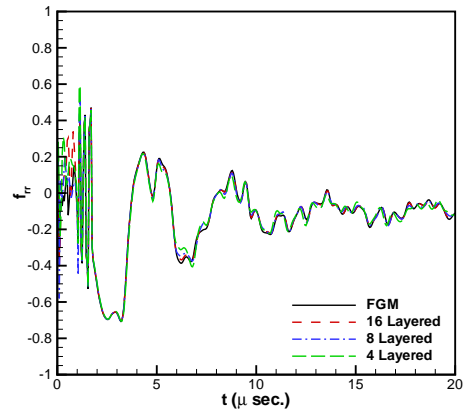


(e)  $z/h = 0.0$

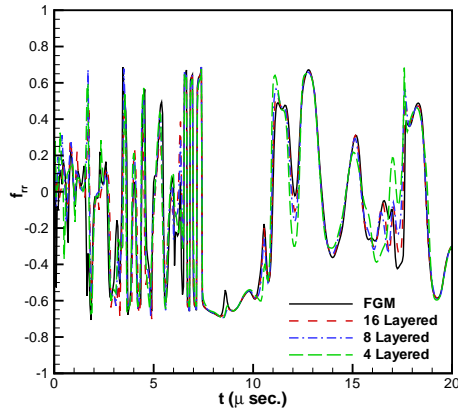
**Figure A.27:**  $f_{rr}$  values at  $r/R = 0.0$ .



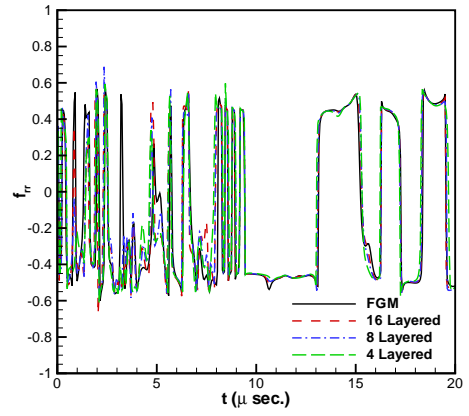
(a)  $r/R = 0.0$



(b)  $r/R = 0.2$

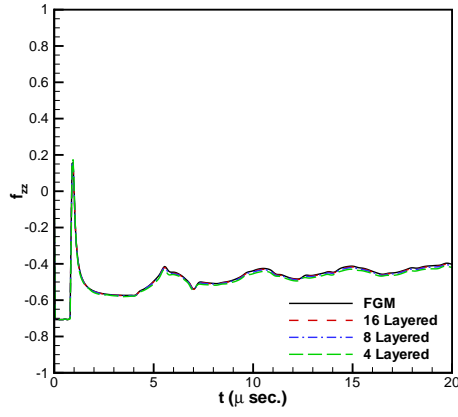


(c)  $r/R = 0.8$

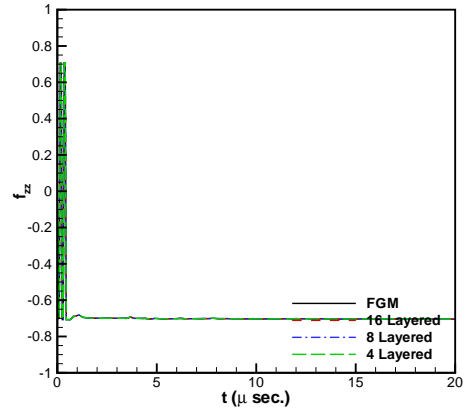


(d)  $r/R = 1.0$

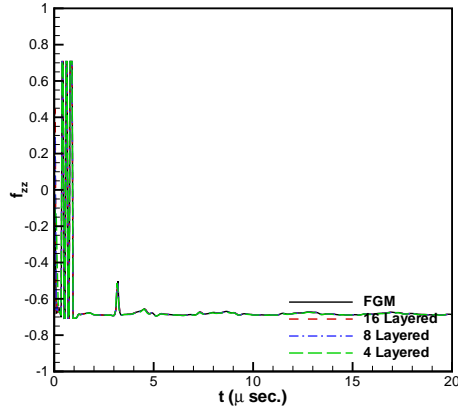
**Figure A.28:**  $f_{rr}$  values at  $z/h = 0.5$ .



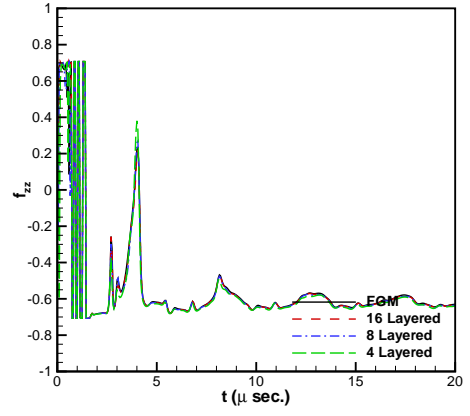
(a)  $z/h = 1.0$



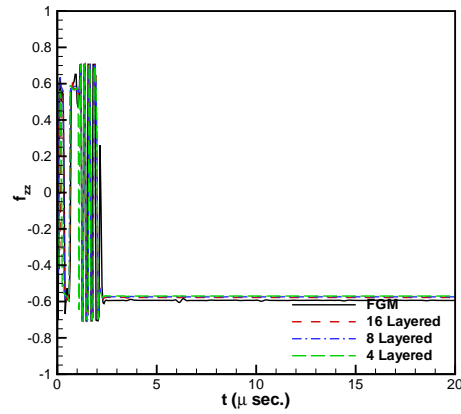
(b)  $z/h = 0.75$



(c)  $z/h = 0.5$

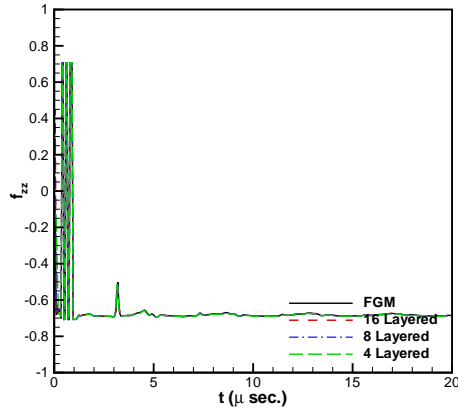


(d)  $z/h = 0.25$

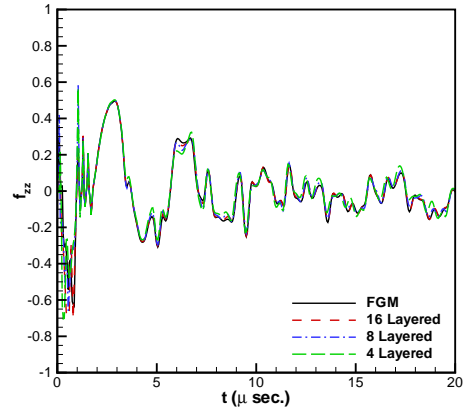


(e)  $z/h = 0.0$

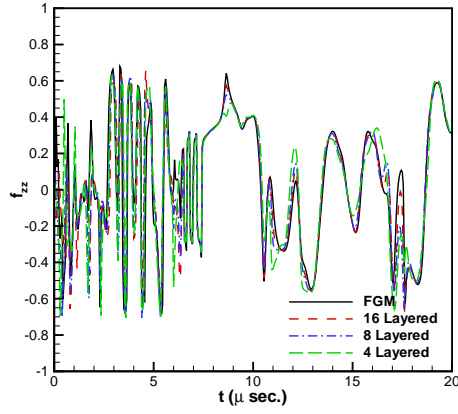
**Figure A.29:**  $f_{zz}$  values at  $r/R = 0.0$ .



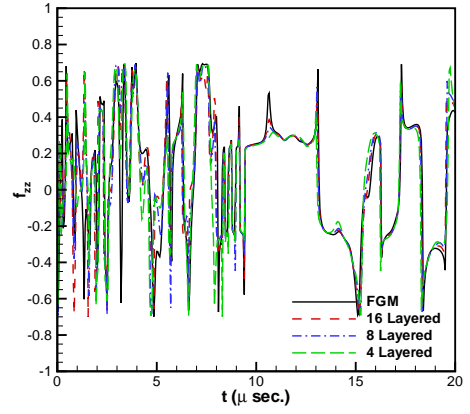
(a)  $r/R = 0.0$



(b)  $r/R = 0.2$

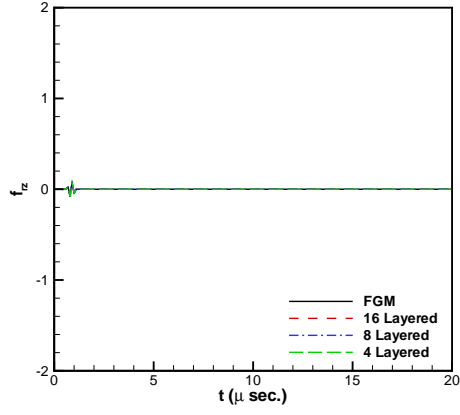


(c)  $r/R = 0.8$

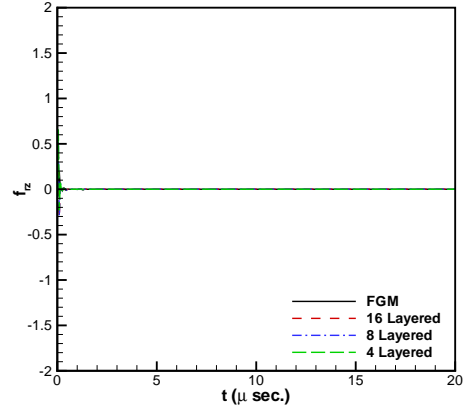


(d)  $r/R = 1.0$

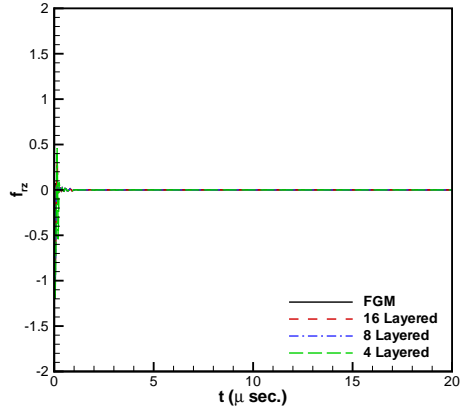
**Figure A.30:**  $f_{zz}$  values at  $z/h = 0.5$ .



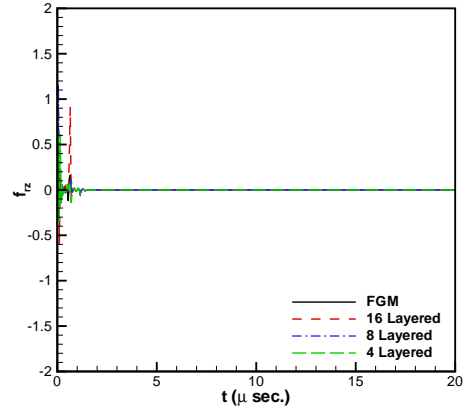
(a)  $z/h = 1.0$



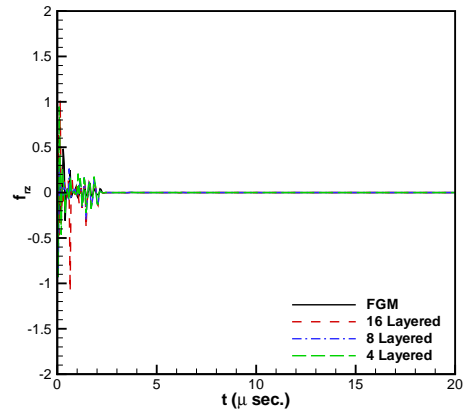
(b)  $z/h = 0.75$



(c)  $z/h = 0.5$

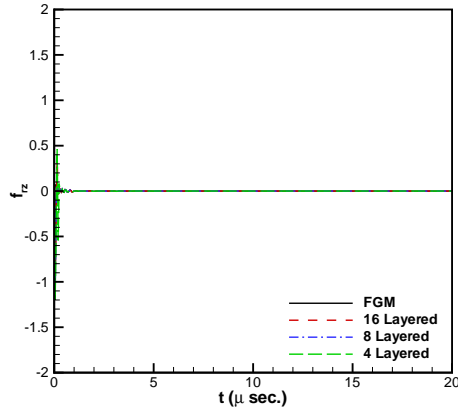


(d)  $z/h = 0.25$

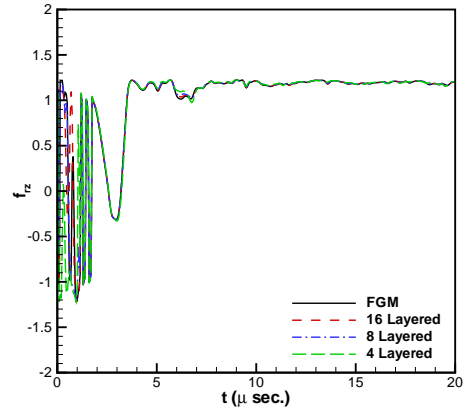


(e)  $z/h = 0.0$

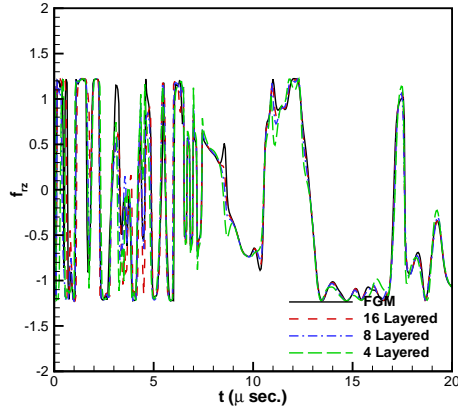
**Figure A.31:**  $f_{rz}$  values at  $r/R = 0.0$ .



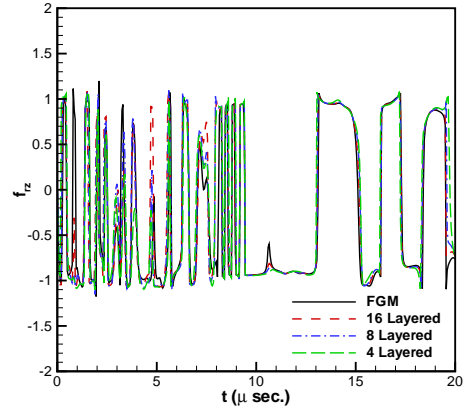
(a)  $r/R = 0.0$



(b)  $r/R = 0.2$



(c)  $r/R = 0.8$



(d)  $r/R = 1.0$

**Figure A.32:**  $f_{rz}$  values at  $z/h = 0.5$ .



(a) FGM Plate at  $t = 5 \mu s$



(b) FGM Plate at  $t = 10 \mu s$



(c) 16 Layered Plate at  $t = 5 \mu s$



(d) 16 Layered Plate at  $t = 10 \mu s$



(e) 8 Layered Plate at  $t = 5 \mu s$



(f) 8 Layered Plate at  $t = 10 \mu s$



(g) 4 Layered Plate at  $t = 5 \mu s$



(h) 4 Layered Plate at  $t = 10 \mu s$

**Figure A.33:** Shear stress in the plate at  $t = 5 \mu sec$  and  $t = 10 \mu sec$ .



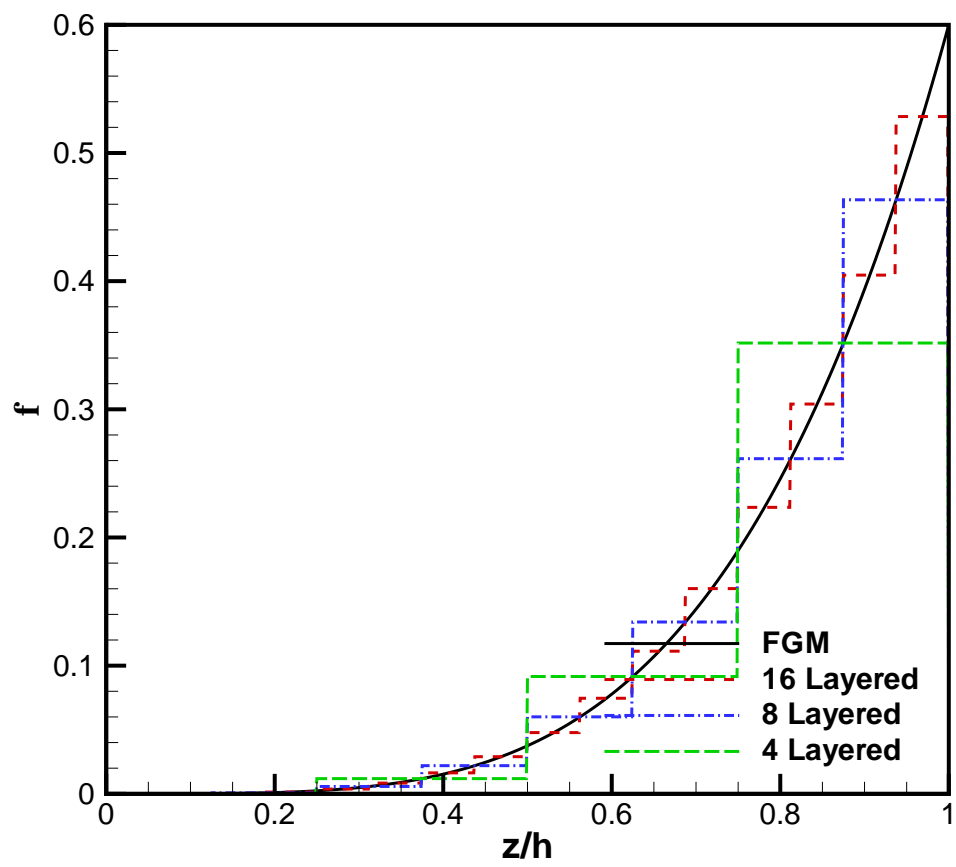
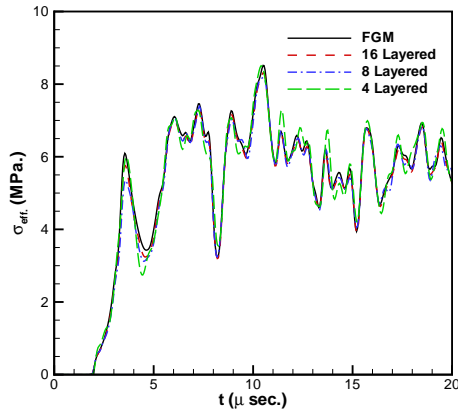
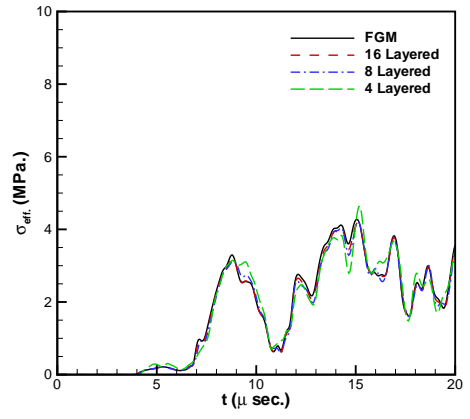


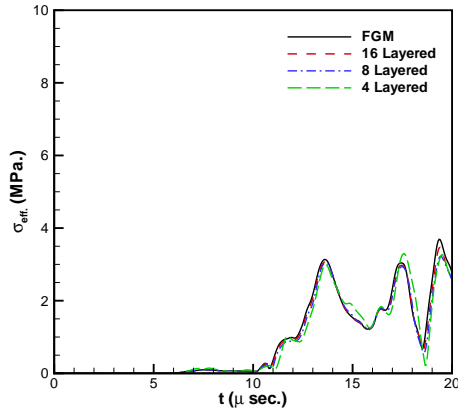
**Figure A.34:** Variation of volume fraction of ceramic phase among the thickness for backward loaded plate.



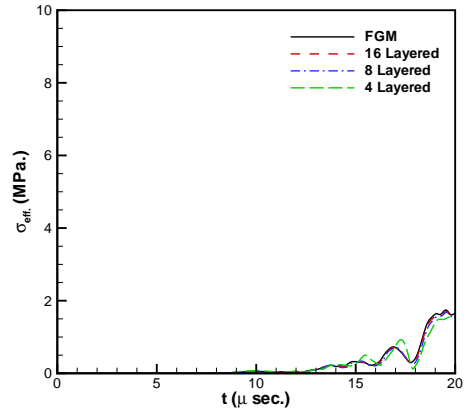
(a)  $r/R = 0.2$



(b)  $r/R = 0.4$

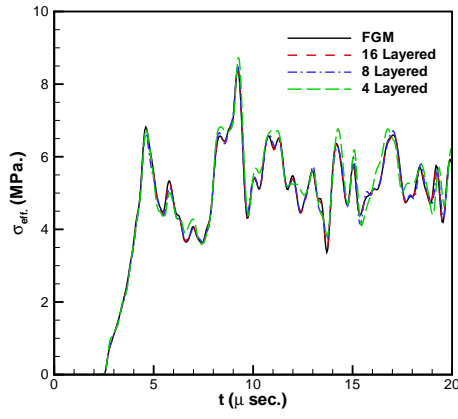


(c)  $r/R = 0.6$

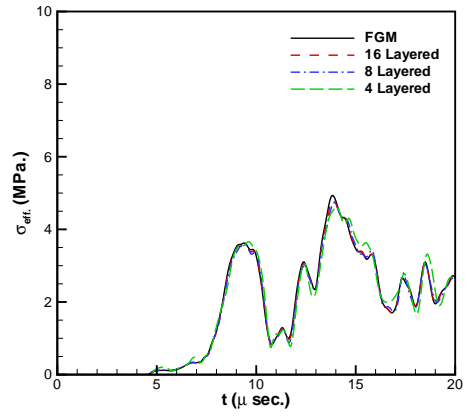


(d)  $r/R = 0.8$

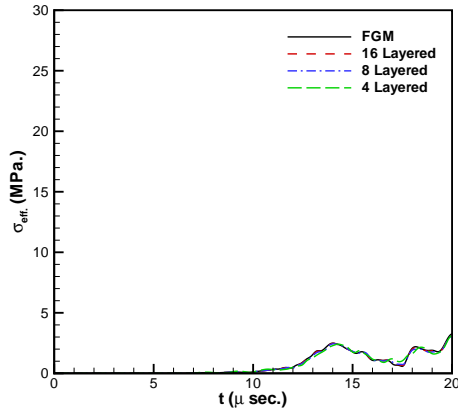
**Figure A.35:** Effective stress along the radius at  $z/h = 0.625$ .



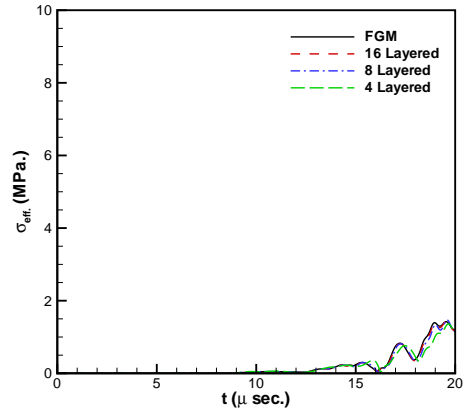
(a)  $r/R = 0.2$



(b)  $r/R = 0.4$

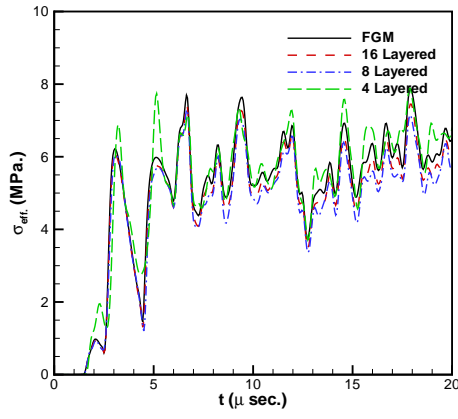


(c)  $r/R = 0.6$

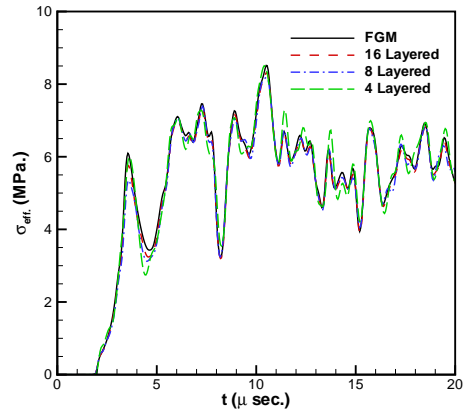


(d)  $r/R = 0.8$

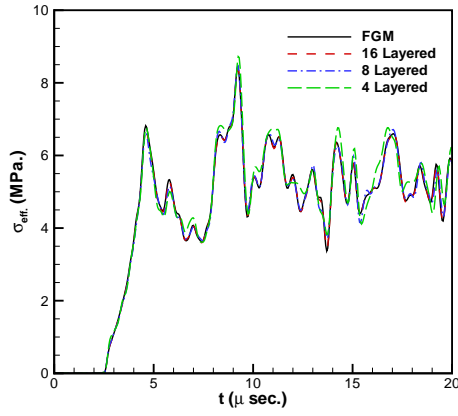
**Figure A.36:** Effective stress among the radius at  $z/h = 0.375$ .



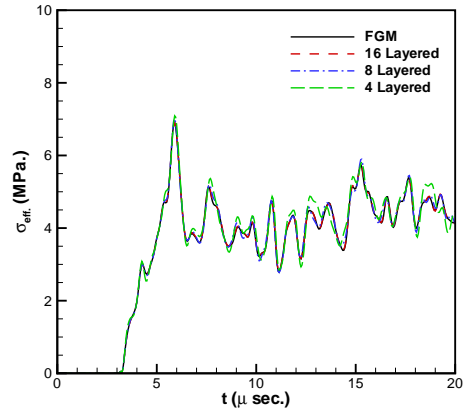
(a)  $z/h = 0.875$



(b)  $z/h = 0.625$

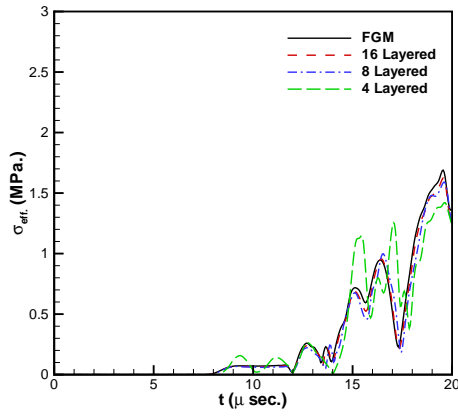


(c)  $z/h = 0.375$

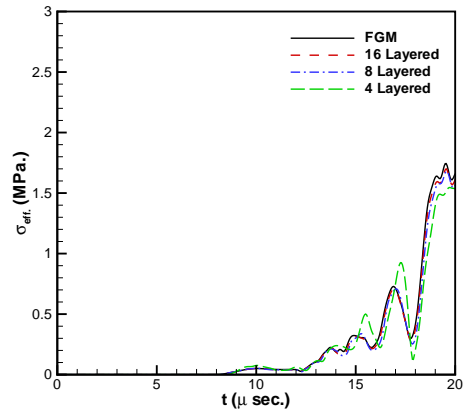


(d)  $z/h = 0.125$

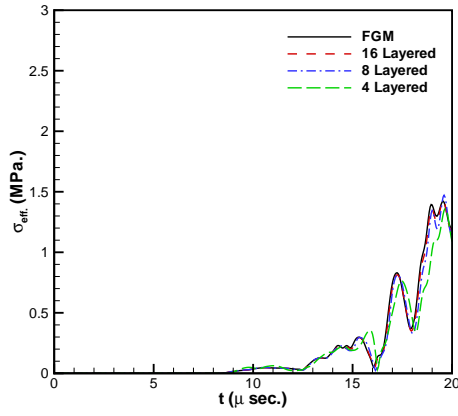
**Figure A.37:** Effective stress along the thickness at  $r/R = 0.2$ .



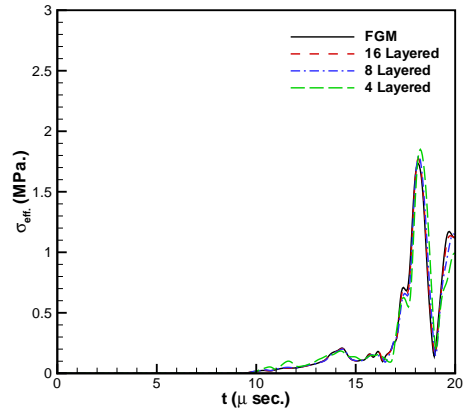
(a)  $z/h = 0.875$



(b)  $z/h = 0.625$

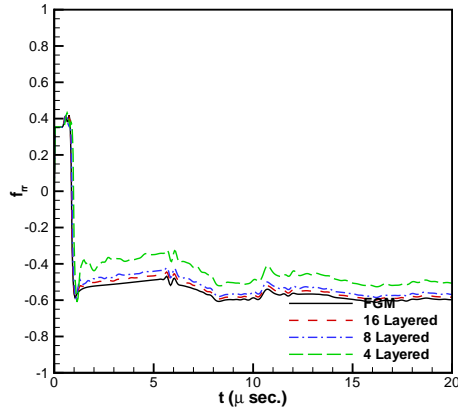


(c)  $z/h = 0.375$

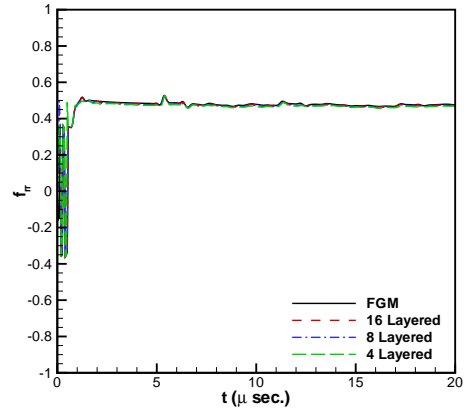


(d)  $z/h = 0.125$

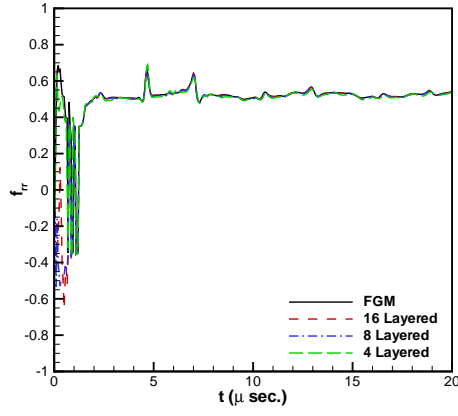
**Figure A.38:** Effective stress among the thickness at  $r/R = 0.8$ .



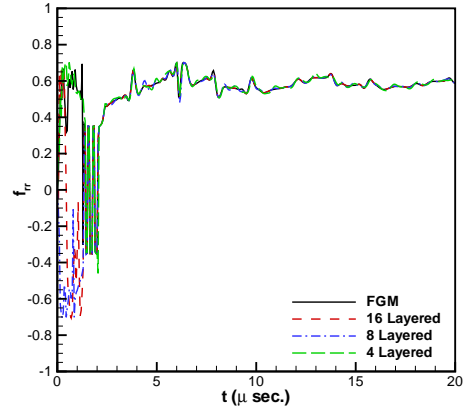
(a)  $z/h = 1.0$



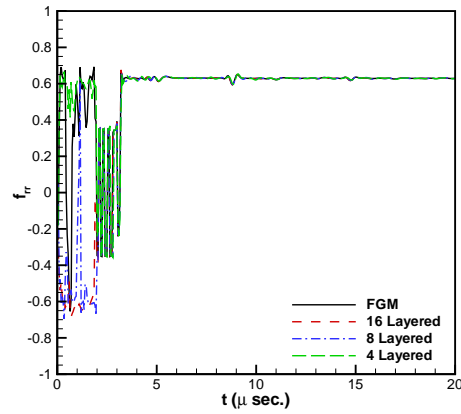
(b)  $z/h = 0.75$



(c)  $z/h = 0.5$

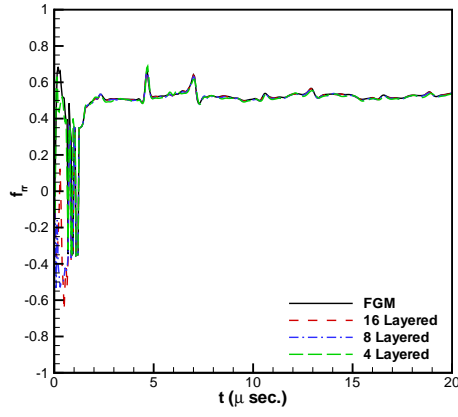


(d)  $z/h = 0.25$

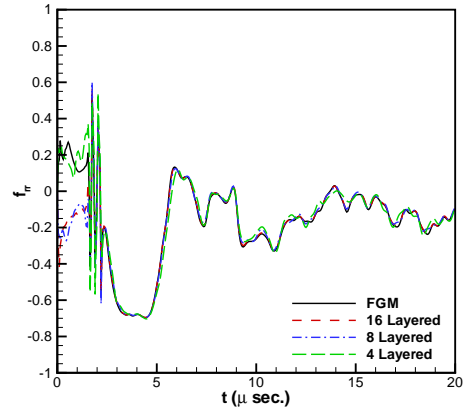


(e)  $z/h = 0.0$

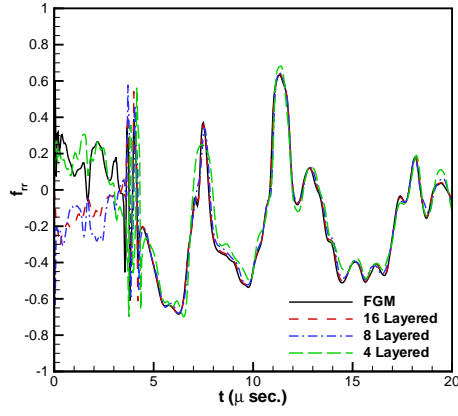
**Figure A.39:**  $f_{rr}$  values at  $r/R = 0.0$ .



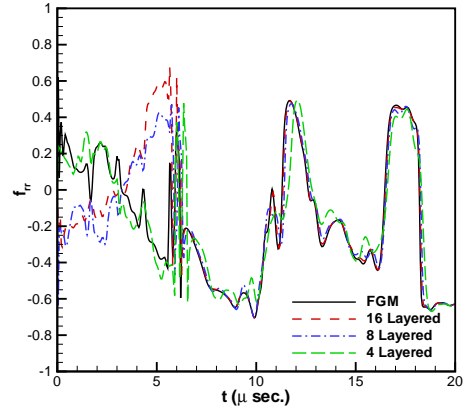
(a)  $r/R = 0.0$



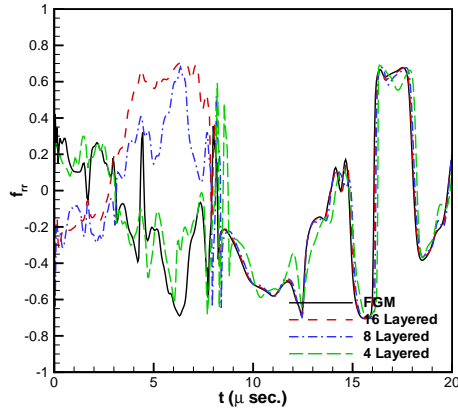
(b)  $r/R = 0.2$



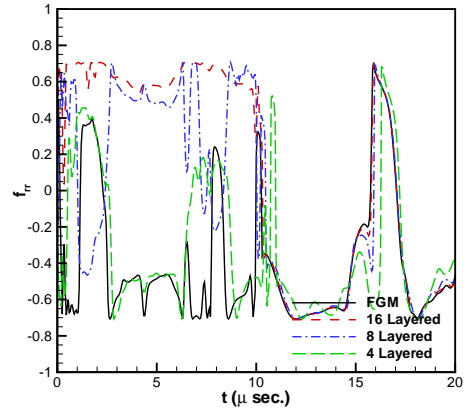
(c)  $r/R = 0.4$



(d)  $r/R = 0.6$

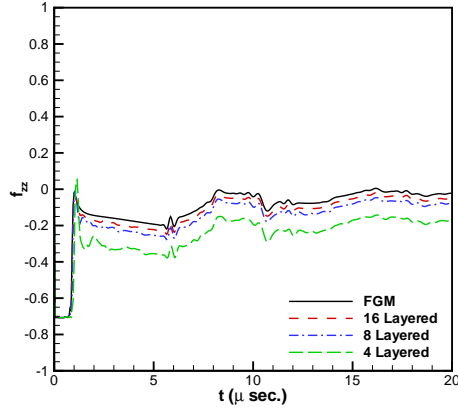


(e)  $r/R = 0.8$

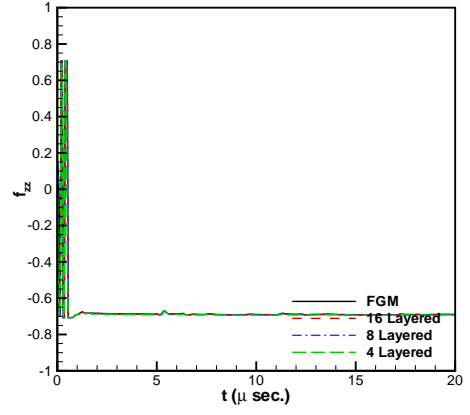


(f)  $r/R = 1.0$

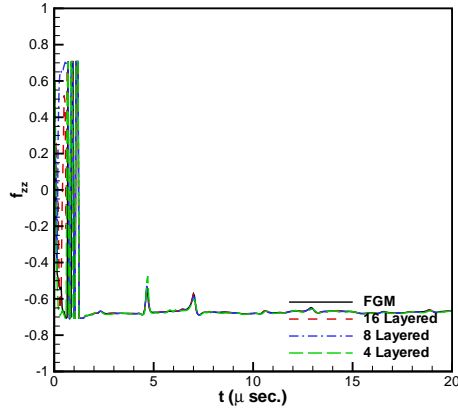
**Figure A.40:**  $f_{rr}$  values at  $z/h = 0.5$ .



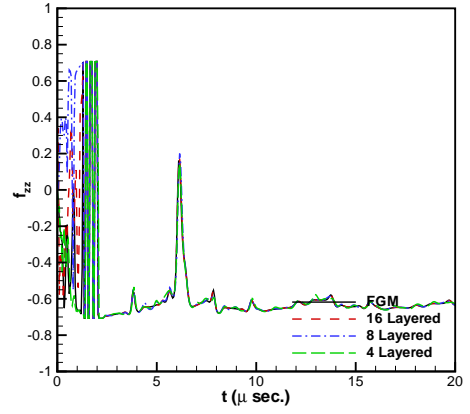
(a)  $z/h = 1.0$



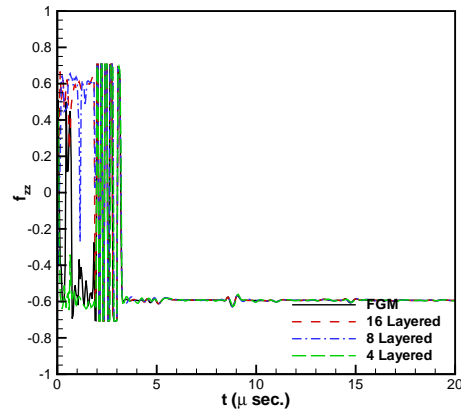
(b)  $z/h = 0.75$



(c)  $z/h = 0.5$



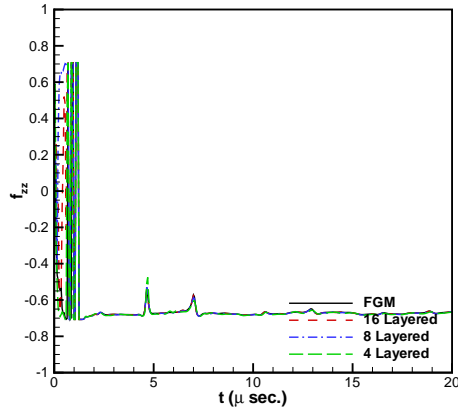
(d)  $z/h = 0.25$



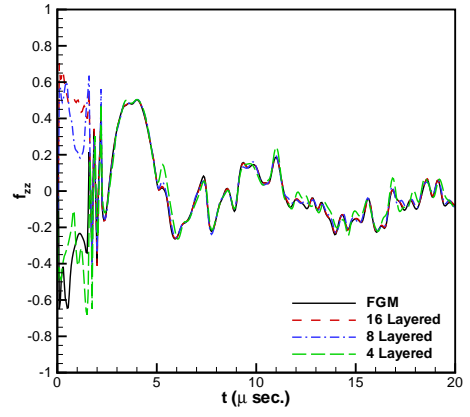
(e)  $z/h = 0.0$

**Figure A.41:**  $f_{zz}$  values at  $r/R = 0.0$ .

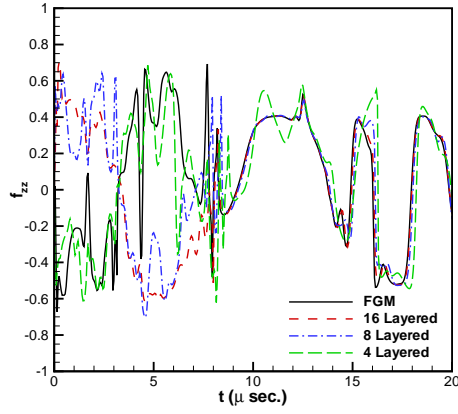




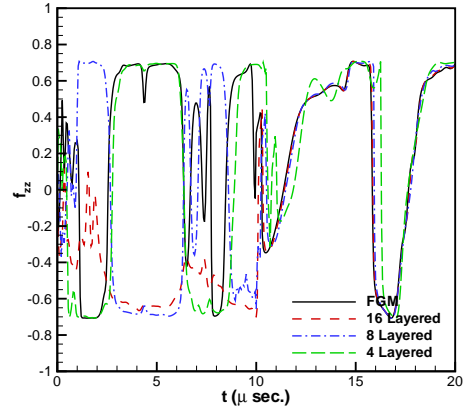
(a)  $r/R = 0.0$



(b)  $r/R = 0.2$

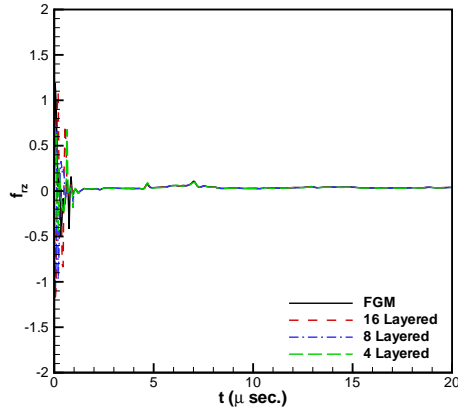


(c)  $r/R = 0.8$

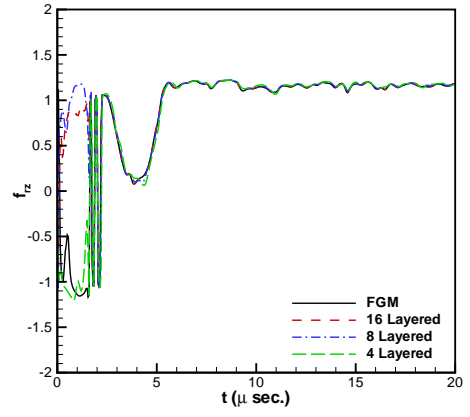


(d)  $r/R = 1.0$

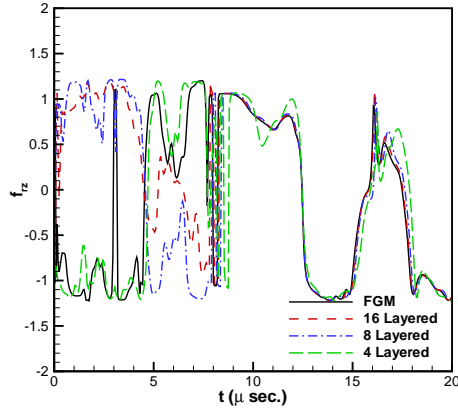
**Figure A.42:**  $f_{zz}$  values at  $z/h = 0.5$ .



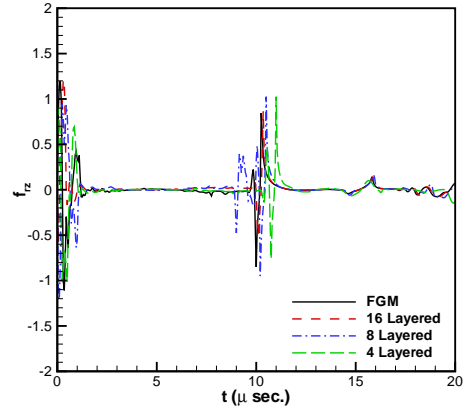
(a)  $r/R = 0.0$



(b)  $r/R = 0.2$



(c)  $r/R = 0.8$



(d)  $r/R = 1.0$

**Figure A.43:**  $f_{rz}$  values at  $z/h = 0.5$ .



(a) FGM Plate at  $t = 5 \mu s$



(b) FGM Plate at  $t = 10 \mu s$



(c) 16 Layered Plate at  $t = 5 \mu s$



(d) 16 Layered Plate at  $t = 10 \mu s$



(e) 8 Layered Plate at  $t = 5 \mu s$



(f) 8 Layered Plate at  $t = 10 \mu s$



(g) 4 Layered Plate at  $t = 5 \mu s$



(h) 4 Layered Plate at  $t = 10 \mu s$

**Figure A.44:** Shear stress in the plate at two different time.

## B. Kinematical Conditions of Compatibility

Let us write the time variation of  $\phi$  on both sides of the singular surface.

$$\frac{\delta\phi^+}{\delta t} = \frac{\partial\phi^+}{\partial t} + \frac{\partial\phi^+}{\partial x_i} \frac{\delta x_i}{\delta t} \quad (\text{B.1})$$

$$\frac{\delta\phi^-}{\delta t} = \frac{\partial\phi^-}{\partial t} + \frac{\partial\phi^-}{\partial x_i} \frac{\delta x_i}{\delta t} \quad (\text{B.2})$$

, where

$$\frac{\delta x_i}{\delta t} = u_n n_i \quad (\text{B.3})$$

Subtracting equation B.2 from equation B.1, one gets the following equation.

$$\frac{\delta[\phi]}{\delta t} = \left[\frac{\partial\phi}{\partial t}\right] + \left[\frac{\partial\phi}{\partial x_i}\right] u_n n_i \quad (\text{B.4})$$

In equation B.4  $u_n$  is the speed of propagation of singular surface. The equation B.4 is first order kinematical condition of compatibility.

If one replaces the  $\phi$  by  $\partial\phi/\partial t$ , second order kinematical condition of compatibility equation is obtained.

$$\frac{\delta[\partial\phi/\partial t]}{\delta t} = \left[\frac{\partial^2\phi}{\partial t^2}\right] + \left[\frac{\partial^2\phi}{\partial x_i \partial t}\right] u_n n_i \quad (\text{B.5})$$

### C. Balance Laws Around Discontinuous Surface

Two fundamental theorems have been used in deriving the local balance laws around a discontinuity surface. One is the Rayleigh transport theorem and later is the Green Gauss theorem. Time rate of change of a volume integral of a variable  $\phi$  can be written as follows.

$$\frac{d}{dt} \int_{\Omega} \phi dv = \int_{\Omega} \left( \frac{\partial \phi}{\partial t} + \nabla(\phi \mathbf{v}) \right) dv + \int_{\Gamma} \phi (\mathbf{v} - \mathbf{v}_s) \cdot \mathbf{n} ds \quad (\text{C.1})$$

, where  $\mathbf{v}_s$  is the velocity and  $\mathbf{n}$  is the unit outward vector of the boundary  $\Gamma$ .

If the material volume contains a discontinuity in  $\phi$ , writing the Rayleigh transport theorem separately for the each side of discontinuity surface and summing them yields the following function, which can be applied to material domains containing discontinuous surfaces.

$$\frac{d}{dt} \int_{\Omega - \Gamma_s} \phi dv = \int_{\Omega - \Gamma_s} \left( \frac{\partial \phi}{\partial t} + \nabla(\phi \mathbf{v}) \right) dv + \int_{\Gamma_s} [\phi (\mathbf{v} - \mathbf{c}) \cdot \mathbf{n}_s] ds \quad (\text{C.2})$$

In Equation (C.2),  $\mathbf{c}$  is the velocity of the singular surface and  $\mathbf{n}_s$  is the unit normal of the singular surface from  $\Omega_-$  to  $\Omega_+$ .

The generalized Green-Gauss theorem for a tensor field  $\boldsymbol{\tau}$  can be written as follows.

$$\int_{\Gamma} \boldsymbol{\tau} \cdot \mathbf{n} ds = \int_{\Omega} \nabla \cdot \boldsymbol{\tau} dv \quad (\text{C.3})$$

Similar to the Rayleigh transport theorem, writing the equation C.3 for domains  $\Omega_-$  and  $\Omega_+$  and summing them yields the following equation.

$$\int_{\Gamma - \Gamma_s} \boldsymbol{\tau} \cdot \mathbf{n} ds = \int_{\Omega - \Gamma_s} \nabla \cdot \boldsymbol{\tau} dv + \int_{\Gamma_s} [\boldsymbol{\tau}] \cdot \mathbf{n}_s ds \quad (\text{C.4})$$

Now let us derive the local balance laws around a discontinuity surface. If we substitute  $\rho$  in place of  $\phi$  in equation C.2, we get the following equation.

$$\frac{d}{dt} \int_{\Omega - \Gamma_s} \rho dv = \int_{\Omega - \Gamma_s} \left( \frac{\partial \rho}{\partial t} + \nabla(\rho \mathbf{v}) \right) dv + \int_{\Gamma_s} [\rho (\mathbf{v} - \mathbf{c})] \cdot \mathbf{n}_s ds \quad (\text{C.5})$$

In equation C.5 first integral on the right side vanishes. Thus the balance laws are satisfied in all parts of the material domain  $\Omega$ . Then continuity equation around a singular surface can be written as follows.

$$[\rho(\mathbf{v} - \mathbf{c})] \cdot \mathbf{n}_S \text{ on } \Gamma_S \quad (\text{C.6})$$

In deriving balance of momentum around a singular surface, we substitute  $\rho \mathbf{v}$  in place of  $\phi$  in equation C.2 and substitute  $\sigma$  in place of  $\tau$  in equation C.4. Then we get the following equation.

$$[\rho \mathbf{v} (\mathbf{v} - \mathbf{c})] \cdot \mathbf{n}_S = [\sigma] \cdot \mathbf{n}_S \text{ on } \Gamma_S \quad (\text{C.7})$$

Energy balance around a discontinuous surface can be obtained similarly as follows.

$$[(\rho \varepsilon + \frac{1}{2} \mathbf{v} \cdot \mathbf{v})(\mathbf{v} - \mathbf{c})] \cdot \mathbf{n}_S = [\sigma \cdot \mathbf{v} - \mathbf{q}] \cdot \mathbf{n}_S \text{ on } \Gamma_S \quad (\text{C.8})$$

, where  $\varepsilon$  is the internal energy per unit volume and  $\mathbf{q}$  is the heat flux.

## **CIRRICULUM VITAE**

Hüseyin Gökmen AKSOY 1976 yılında Aksaray’da doğdu. 1994 yılında kazandığı İ.T.Ü. Makina Fakültesi Makina Mühendisliği Bölümü’nden 1998 yılında mezun oldu. 1998 yılında İ.T.Ü. Fen Bilimleri Enstitüsü’nde başladığı yüksek lisans eğitimini 2001 yılında tamamladı. 2001 yılında başladığı von Karman Akışkanlar Mekaniği Enstitüsü diploma programını 2002 yılında tamamladı. 2003 yılında İstanbul Teknik Üniversitesi Fen Bilimleri Enstitüsünde Doktora öğrenimine başladı.